https://doi.org/10.5194/egusphere-2026-3680
Preprint. Discussion started: 4 September 2026

PyBacktrack 1.5: A community tool for reconstructing paleobathymetry of drill sites, geohistory and global paleobathymetry

R. Dietmar Müller[1], John Cannon[1], Simon Williams[2,1], Adriana Dutkiewicz[1] and Nicky M. Wright[1]

[1]*EarthByte Group, School of Geosciences, University of Sydney, Sydney, NSW 2006, Australia*

[2] *Institute for Marine and Antarctic Studies, University of Tasmania, Hobart, TAS, Australia,*

Correspondence to: R. Dietmar Müller (dietmar.muller@sydney.edu.au)

Abstract

PyBacktrack is a Python community software package that reconstructs the paleo-water depth (paleobathymetry) of ocean drill sites and industry wells through time by combining a model of tectonic subsidence with sediment decompaction and isostatic correction. Since the release of pyBacktrack 1.0, the software has undergone substantial development that culminates in pyBacktrack 1.5. The package now (i) runs on Python 3 and is distributed via the Python Package Index, conda-forge and Docker; (ii) includes a new paleobathymetry gridding module that reconstructs and backtracks all submerged present-day crust through geological time to produce time-dependent paleobathymetry grids; (iii) uses an updated default oceanic age-to-depth model, a globally complete set of rift start/end age grids derived from a deforming plate model, an updated total sediment thickness grid and an updated present-day age grid; (iv) supports both mantle and paleomagnetic reference frames and allows the gridded paleobathymetry to be optionally merged with externally produced paleobathymetry on synthetic, subducted crust; and (v) ships with expanded sea-level model and dynamic topography model libraries. We illustrate pyBacktrack 1.5 with three applications: (1) paleobathymetry reconstructions since the Early Cretaceous of the North Atlantic and the Southern Ocean; (2) one-dimensional backstripping and geohistory analysis at a long-record industry well on the Australian North West Shelf in three configurations (including or omitting eustatic sea level, and including a joint sea level and dynamic topography correction); and (3) a margin-scale gridded tectonic-subsidence-rate analysis of 109 Australian Northwest Shelf industry wells, quantifying how much of the inferred tectonic subsidence rate is dependent on eustatic and dynamic-topographic corrections in space and time. Together, these developments make pyBacktrack 1.5 a more accessible, extensible and globally applicable framework for reconstructing paleobathymetry and testing the tectonic, sedimentary, sea-level and dynamic-topographic controls on basin evolution.

1. Introduction

Paleobathymetry, the past water depth of seafloor or continental margin locations, is a fundamental boundary condition for reconstructing the long-term evolution of ocean basins, continental margins, marine gateways, ocean circulation and the carbon cycle. The bathymetry at any site of marine sedimentation changes through time in response to several superimposed processes, including thermal subsidence of oceanic and rifted continental crust, compaction-driven progressive porosity reduction of the sediment column, isostatic adjustment to the changing sediment load, mantle-flow driven dynamic topography, and eustatic sea-level change (Allen and Allen, 2005; Müller et al., 2018). Quantitative recovery of paleobathymetry at a drill site or in a basin therefore demands an integrated workflow that brings these processes together in a single, reproducible framework.

https://doi.org/10.5194/egusphere-2026-3680
Preprint. Discussion started: 4 September 2026

Beyond its role in basin analysis, paleobathymetry is a first-order boundary condition for the broader community that models the deep-time Earth system. In paleoclimate and paleoceanographic simulations, the depth and width of marine gateways, the location and depth of mid-ocean ridges, and the elevation of submarine plateaus together control the geometry of the major ocean basins, the routes available to deep and intermediate water masses, and the partitioning of meridional and zonal flow (Hutchinson et al., 2018; Lunt et al., 2021; Sauermilch et al., 2021; Sijp et al., 2014). Paleobathymetry sets the position of the carbonate compensation depth (CCD), modulates organic-carbon burial efficiency and the storage of dissolved inorganic carbon (Pälike et al., 2012; Crampton et al., 2018; Dutkiewicz and Müller, 2022), and thereby couples solid-Earth tectonics to the long-term carbon cycle (Müller et al., 2022). It determines which shelves are flooded and which are emergent, which in turn controls biogeographic dispersal corridors, marine connectivity, productivity patterns and the extent of epicontinental seas (Allen and Allen, 2005; Kocsis and Scotese, 2020; Poblete et al., 2021). It is also the geometry on which mantle-flow simulations of dynamic topography are tested and compared (Gurnis, 1993; Müller et al., 2017; Braz et al., 2021). For all of these applications time-dependent paleobathymetry grids are required.

PyBacktrack (Müller et al., 2018) is an open-source Python package that implements such a workflow. It provides depth backtracking on both oceanic and continental crust, a library of compaction relationships for common marine lithologies, and a treatment of mantle-flow-derived dynamic topography drawn from a curated bundle of global models. Other open-source tools address related problems, but with different design priorities. For example, PALEOSTRIP is a MATLAB, GUI-based tool designed for user-controlled 1-D, 2-D and 3-D paleobathymetric backtracking, with a particular emphasis on 2-D and 3-D flexural isostasy for mapped stratigraphic surfaces, seismic transects and basin-scale sensitivity tests (Colleoni et al., 2021). PyBacktrack, by contrast, is built around reproducible Python workflows that are directly linked to plate reconstructions, global oceanic and continental subsidence models, dynamic topography corrections and the generation of time-dependent paleobathymetry grids. A central design choice of pyBacktrack, retained in 1.5, is that the tool exposes the underlying physical model as a transparent, modular Python application rather than as a closed-form executable. Every lithology, every sea-level curve and every dynamic-topography model is either a bundled text/NetCDF file or a user-supplied file. This makes pyBacktrack a useful pedagogical and exploratory tool as well as a production research instrument: users can substitute alternative tectonic-subsidence relationships or compaction laws without modifying the core algorithms. PyBacktrack 1.5 preserves and extends this design philosophy.

In the seven years since the 1.0 release, three developments have made a substantial revision of pyBacktrack desirable. First, the broader plate-tectonic modelling community has migrated to Python 3 and to richer, deformation-aware global plate models (e.g., Müller et al., 2019; Cao et al., 2021; Zahirovic et al., 2022). Second, the observational underpinnings of pyBacktrack, including present-day ocean-floor age grids, global total sediment thickness grids and oceanic age–depth relationships, have been refined (Straume et al., 2019; Seton et al., 2020; Richards et al., 2020). Third, a recurring request from users has been to use pyBacktrack to generate not only the depth history of a single site but two-dimensional, time-dependent paleobathymetry grids over entire ocean basins.

PyBacktrack 1.5 addresses these needs. We have ported the package to Python 3, integrated up-to-date age and sediment-thickness grids and an updated default oceanic age-to-depth model (Richards et al., 2020). We have added a paleobathymetry gridding module that reconstructs every present-day submerged grid point back through time, decompacts its sediment column at each reconstruction time and (optionally) merges the result with externally generated paleobathymetry on synthetic, since-subducted crust. We have made the rift start/end age grids,

https://doi.org/10.5194/egusphere-2026-3680
Preprint. Discussion started: 4 September 2026

that underpin the continental subsidence model, globally complete and have based them on the Zahirovic et al. (2022) deforming plate model. PyBacktrack 1.5 is distributed through the Python Package Index, conda-forge and a Docker image; example data, notebooks and a fully documented application programming interface are available at pybacktrack.readthedocs.io. Selected paleobathymetry grid sets are distributed via the EarthByte GPlates data repository and are linked from the pyBacktrack 1.5 documentation. This paper documents the new and updated features in pyBacktrack 1.5 and demonstrates how they can be applied.

2 PyBacktrack 1.5 architecture

The pyBacktrack package consists of several modules that can be either called from the command line as built-in scripts (using `python -m pybacktrack.<module>_cli`) or imported into user Python code for finer-grained control. The four modules are:

1) `backtrack` — reconstructs paleo-water depth at a single drill site, given a stratigraphic file of lithologies and ages and a chosen tectonic-subsidence model. Used for sites where the present-day water depth is known but the paleo-water depths are not.
2) `backstrip` — recovers tectonic subsidence at a single passive-margin site from a stratigraphic file that includes minimum and maximum estimates of paleo-water depth (typically derived from benthic microfossil assemblages). Used to isolate the tectonic contribution to subsidence.
3) `paleo_bathymetry` — new in pyBacktrack 1.4 and substantially extended in 1.5, this module generates two-dimensional, time-dependent paleobathymetry grids by reconstructing every present-day submerged grid point back through time and applying the same physics as the one-dimensional backtrack workflow.
4) `age_to_depth` — converts ocean-floor age to ocean-basement depth using one of three bundled relationships (RHCW18 (Richards et al., 2020), GDH1 (Stein and Stein, 1992) or Crosby_2007 (Crosby, 2007).

These modules are supported by utility modules that expose sediment decompaction routines, sea-level and dynamic-topography samplers and stratigraphic depth-to-age conversion (new since 1.0). They are configured by a bundle of data shipped with the package: lithology definitions, a present-day age and bathymetry grid, a total sediment thickness grid, a crustal thickness grid, dynamic-topography model grids, sea-level curves and the reconstruction model (rotation files and static polygons).

A new utility module `stratigraphic_depth_to_age` has been added in the 1.x series. It interpolates the ages of user-specified stratigraphic depths from a piecewise-linear age–depth model. The `age_to_depth` module has been generalised to accept user-supplied age–depth tables and additional bundled models. The `interpolate` script of pyBacktrack 1.0 remains available and unchanged. Both new modules are available as command-line scripts and as Python functions.

PyBacktrack's physical model is unchanged in 1.5 relative to 1.0. On oceanic crust, the tectonic subsidence at a site is computed from a user-selected age-depth relationship together with the present-day unloaded basement depth (water depth minus an isostatic correction for the present-day sediment thickness). On continental crust, tectonic subsidence is modelled with a McKenzie-style uniform-stretching model (McKenzie, 1978) in which the syn-rift and post-rift subsidence is determined from the present-day sediment thickness and from the rift start and end ages, following Jarvis and McKenzie, 1980). Decompaction of the sediment column at each time step uses the porosity–depth relationships from Müller et al. (2018).

https://doi.org/10.5194/egusphere-2026-3680
Preprint. Discussion started: 4 September 2026

3 New features and improvements since pyBacktrack 1.0

PyBacktrack 1.5 inherits all features of the 1.0 release but introduces numerous additions, replaces several default models with more recent alternatives and changes the installation footprint. We group the changes thematically below. Where a change was first introduced in an earlier 1.x release we indicate the version explicitly.

3.1 Python 3, packaging and installation

PyBacktrack 1.0 supported only Python 2.7, which has been end-of-life since 2020. PyBacktrack 1.5 supports Python 3.8 and above, and depends on pyGPlates (Mather et al., 2024). The package is now installable from the Python Package Index (`pip install pybacktrack`), from conda-forge (`conda install -c conda-forge pybacktrack`) and as a Docker image (`earthbyte/pybacktrack`). Example data, example drill sites and five Jupyter notebooks (backstrip, backtrack, geohistory_analysis, paleobathymetry and reconstruct_drill_sites_on_paleobathymetry) are bundled in a separate, optional install step (`python -c "import pybacktrack; pybacktrack.install_examples()"`). A separate `install_supplementary` script bundles supplementary tooling including the `generate_rift_grids.py` script used to regenerate the built-in rift grids. The continuous-integration test suite runs on Linux, macOS and Windows with all supported Python versions on every push, and the documentation is rebuilt automatically on each commit at pybacktrack.readthedocs.io.

PyBacktrack 1.5 has been refactored around `pyproject.toml`-driven modern packaging, allowing automated wheel builds and SCM-driven versioning. The new packaging removes the need for users to install the dependency library pyGPlates manually, since both PyPI and conda-forge now distribute pyGPlates for the major platforms. As a result, a fresh install of pyBacktrack 1.5 on Linux, macOS or Windows is a one-line `pip install pybacktrack` operation.

3.2 New paleobathymetry gridding module

A prominent addition in pyBacktrack 1.4 and 1.5 is the `paleo_bathymetry` module. Where the original 1.0 release backtracked single one-dimensional drill sites, `paleo_bathymetry` generates two-dimensional paleobathymetry grids by treating every submerged grid point at present day as a virtual drill site. At each user-selected grid spacing (default 6 arc-minutes), a single lithology (default `Average_ocean_floor_sediment`; previously `Shale`) is assigned an initial compacted thickness from the total sediment thickness grid and is progressively decompacted back through time. Loading the decompacted thickness onto the modelled tectonic subsidence (oceanic where the grid point lies inside the age grid, continental where it does not) together with optional dynamic topography and sea-level contributions yields a paleo-water depth at each grid point and each reconstruction time. Each grid point is reconstructed using a global plate model and the reconstructed locations, together with their paleo-water depths, are interpolated onto a regular output grid at every output time.

Trench-adjacent grid points produce spuriously deep paleobathymetry when reconstructed back into accreted forearc settings. To suppress this artefact, pyBacktrack 1.5 ships with a per-trench exclusion mask that omits, by default, present-day grid points within 60 km of the subducting plate side of each trench. The exclusion distances were hand-tuned for each trench based on the resultant paleobathymetry and can be over-ridden by the user with `--exclude_distances_to_trenches_kms`.

The module further supports merging the pyBacktrack-derived grids with externally produced paleobathymetry on synthetic (now-subducted) crust. Because pyBacktrack only generates

https://doi.org/10.5194/egusphere-2026-3680
Preprint. Discussion started: 4 September 2026

paleobathymetry for crust that persists at present day, the merging operation fills the inevitable gaps over the former Pacific, Tethys and Neo-Tethys oceans. The traditional paleobathymetry workflow used to fill these gaps is described by Wright et al. (in prep.).

3.3 Updated default oceanic age-to-depth model

The default age-to-depth model was updated in pyBacktrack 1.4 from GDH1 (Stein and Stein, 1992) to the plate model of Richards et al. (2020; "RHCW18"). The preferred RHCW18 parameters used by pyBacktrack are a mantle potential temperature of 1333 °C, a plate thickness of 130 km and a zero-age ridge depth of 2500 m. Both GDH1 and the Crosby (2007) model remain available via the `-m` command-line option. RHCW18 was selected as the default because it more accurately reproduces depth–age data on undeformed seafloor that has not been thermally rest older than ~80 Myr than GDH1 (Richards et al., 2020) and yields global oceanic depth residuals that are more nearly isotropic with respect to age and plate identity (Hoggard et al., 2017; Richards et al., 2018). However, much of the preserved seafloor underlain by ocean crust has been thermally rejuvenated by volcanism, reheating and shallowing (Stein and Stein, 1992). Therefore, depending on the user's preferences or applications, GDH-1 often remains a viable choice.

3.4 Updated reconstruction model and reference-frame support

The default plate reconstruction model used by `paleo_bathymetry` in pyBacktrack 1.5 is Zahirovic et al. (2022), replacing the Müller et al. (2019) model used in 1.4 and earlier. The two models are nearly identical for the period 0–250 Ma; the Zahirovic et al. (2022) model additionally incorporates South China deformation from Cao et al. (2021), which produces a slightly different optimised mantle reference frame for that interval. PyBacktrack 1.5 supports any plate reference frame, including mantle reference frames (often expressed by anchor plate 0, the default) and the paleomagnetic reference frame of Zahirovic et al. (2022), here expressed by anchor plate 701701; the paleomagnetic frame is preferred for paleoclimate-related research. Users may supply their own static polygons and rotation files via the `--static_polygon_filename` and `--rotation_filenames` options; only the present-day grid-point reconstruction is affected — the dynamic-topography sampling uses each model's own internal reconstruction.

3.5 Globally complete rift start/end age grids

PyBacktrack's continental subsidence model requires the rift start and end ages at each location. PyBacktrack 1.0 obtained these from the drill-site file. PyBacktrack 1.4 introduced built-in rift start/end age grids generated from the Müller et al. (2019) deforming plate model, restricted to present-day submerged continental crust. In 1.5 the rift grids have been regenerated from the Zahirovic et al. (2022) deforming model and, crucially, extended to global coverage: every grid point that is not on actively deforming continental crust inherits the rift start and end ages of its nearest deforming grid point. This decouples the rift grids from the default age grid and from the default total sediment thickness grid, so that paleobathymetry can be regenerated with alternative grids (for example, a user-supplied age grid with a slightly different continent–ocean boundary, or a sediment thickness grid with a slightly different coastline) without leaving sliver gaps at grid boundaries. The script that generates the rift grids — `generate_rift_grids.py` in pybacktrack/supplementary — is documented in the user manual and can be rerun for any user-supplied deforming plate model.

3.6 Updated default age and sediment-thickness grids, lithology and sea level curves

The default present-day age grid was updated in pyBacktrack 1.4 from the Müller et al. (2008) compilation to the 6 arc-minute compilation of Seton et al. (2020), which uses the Gee and Kent (2007) timescale and incorporates the seafloor-spreading parameters of Müller et al. (2016b) and Wright et al. (2016). The default total sediment thickness grid was updated in pyBacktrack 1.4 from the NOAA NGDC 5 arc-minute compilation to GlobSed (Straume et al., 2019), which provides a more accurate global compilation of sediment thicknesses with substantially improved coverage of high-latitude oceans. The bundled lithology library in pyBacktrack consists of two files. The "primary" file (16 entries) provides the porosity–depth relations for the lithologies tabulated in Müller et al. (2018) and remains unchanged. The "extended" file in pyBacktrack 1.5 ships 11 additional lithologies including anhydrite, chert, conglomerate, dolostone, grainstone, mafic igneous rocks, marl, organic mud, reef carbonate, rhyolite, salt and tuff. Users may continue to supply their own lithology definitions via the `-l` option. PyBacktrack 1.5 ships several bundled sea-level curves: the standard and long-term curves of Haq et al. (1987), Miller et al. (2020) and a composite curve of three published curves by Haq and Ogg (2024) (0–66 Ma), Haq (2014) (66-140 Ma) and Haq (2017) (140.1-205 Ma).

4 Application examples

We illustrate pyBacktrack 1.5 with three complementary applications. The new paleobathymetry-gridding workflow is the single most novel addition since version 1.0, and we present it as a reproducible flowchart (Fig. 1). We illustrate its products with time-dependent paleobathymetry maps of the North Atlantic Ocean (Fig. 2) and the Southern Ocean (Fig. 3), and benchmark the released grids (Fig. 4) against the independent Straume et al. (2020) Cenozoic forward model. We apply the pyBacktrack workflow for individual drill sites to a regional, well-constrained passive margin, the Australian North West Shelf, where we (i) map the well coverage on a vertical-gravity-gradient basemap (Fig. 5), (ii) show the long-term sea-level and dynamic-topography time series that drive the corrections at the featured well asteras (Fig. 6), (iii) demonstrate one-dimensional backstripping at that single long-record well in three configurations (Fig. 7), (iv) present a geohistory ("Wheeler") diagram for the same well (Fig. 8), and (v) generalise the workflow to margin-scale gridded tectonic-subsidence rates across all 109 wells (Figs. 9-12). All figure scripts are bundled with the paper in `figures/scripts/`. Figures 1, 4, 5, 6, 7, 8, 9, 10, 11 and 12 are produced with pyGMT or matplotlib (Uieda et al., 2024); Figures 2 and 3 follow the canonical plotting pattern of the bundled pyBacktrack notebook `reconstruct_drill_sites_on_paleobathymetry.ipynb` (matplotlib + cartopy + `gplately.Raster` + `gplately.PlotTopologies` (Mather et al., 2024)).

4.1 Paleobathymetry-gridding workflow

The most novel addition in pyBacktrack 1.5 - relative to pyBacktrack 1.0 (Müller et al., 2018) - is the module that generates time-dependent two-dimensional paleobathymetry grids by reconstructing and backtracking every present-day submerged grid point. The workflow integrates the original 1.0 one-dimensional physics (oceanic and continental subsidence, sediment decompaction, sea-level correction, dynamic-topography correction) with three new building blocks: (i) globally complete rift start/end age grids; (ii) plate reconstruction of every grid point using a user-selected deforming plate model (default Zahirovic et al., 2022); and (iii) optional merging with externally generated forward-modelled paleobathymetry on synthetic, since-subducted crust. Figure 1 summarises the data flow and the algorithmic steps.

https://doi.org/10.5194/egusphere-2026-3680
Preprint. Discussion started: 4 September 2026

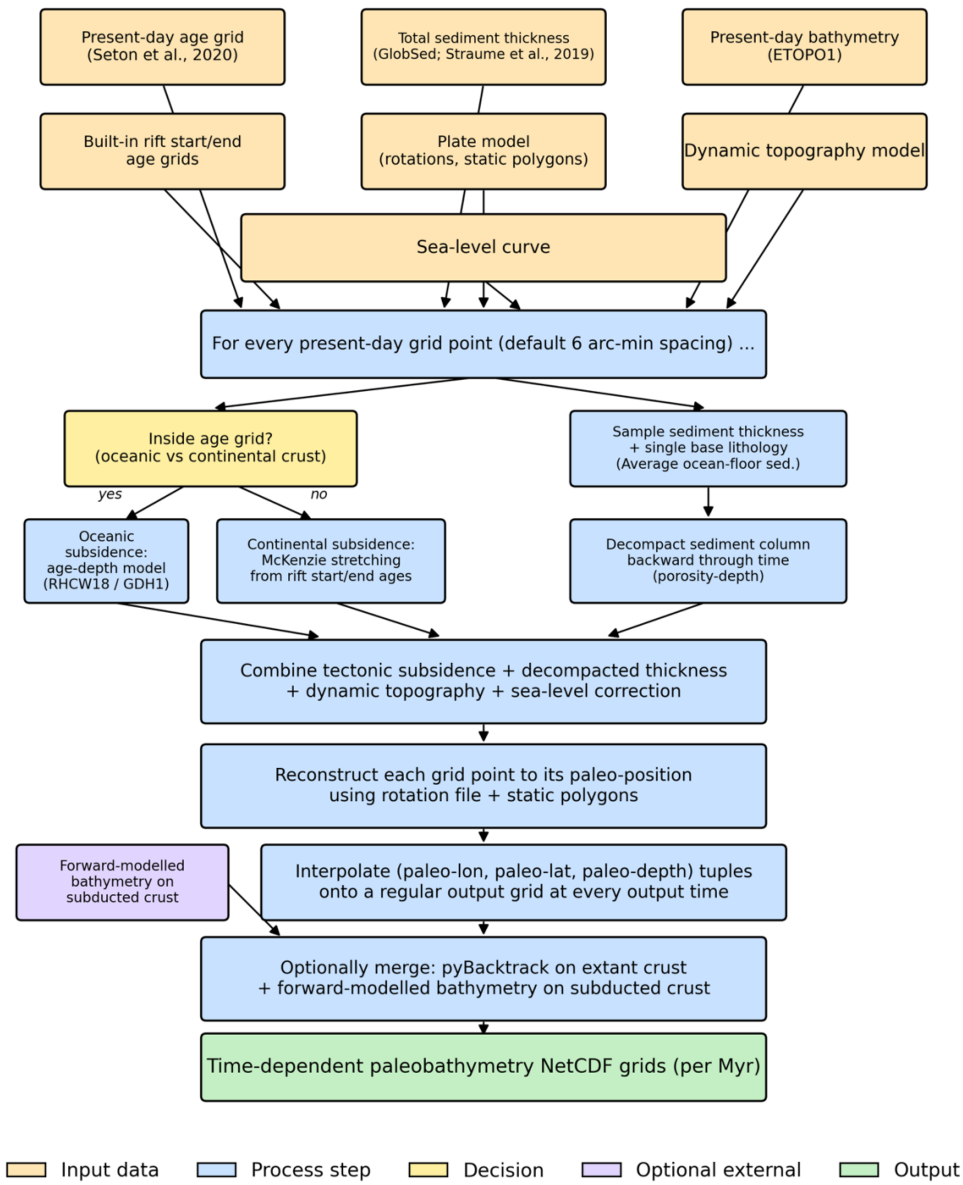

Figure 1. *pyBacktrack 1.5 paleobathymetry-gridding workflow. Peach boxes are input data (present-day age, sediment thickness, bathymetry; rift start/end age grids; plate model; dynamic-topography model; sea-level curve). Blue boxes are processing steps (decompaction; oceanic/continental subsidence; plate reconstruction; grid interpolation). The yellow box is the per-grid-point decision between oceanic and continental crust based on the oceanic crustal age grid used. The lavender box is the optional traditional-paleobathymetry input for*

https://doi.org/10.5194/egusphere-2026-3680
Preprint. Discussion started: 4 September 2026

subducted crust (involving grid merging). The green box is the final output as NetCDF paleobathymetry grids.

Each grid point at present day (default 6 arc-min spacing) is classified as oceanic (inside the present-day age grid) or continental (outside). Oceanic points use a user-selected age-depth model (default RHCW18) to compute tectonic subsidence at every reconstruction time. Continental points use a McKenzie-style uniform-stretching model parameterised by the rift start and end ages sampled from the built-in rift grids. Each point is assigned an initial compacted sediment thickness from the GlobSed total-sediment-thickness grid (Straume et al., 2019) and a single base lithology (default `Average_ocean_floor_sediment`). The column is decompacted backward through time using the porosity-depth relationship of the base lithology, and the decompacted thickness is combined with the modelled tectonic subsidence and the optional dynamic-topography and sea-level contributions to obtain a paleo-water depth at every reconstruction time. Each present-day grid point is then reconstructed to its paleo-position using the plate model, and the resulting (paleo-lon, paleo-lat, paleo-water depth) tuples are interpolated onto a regular output grid at every output time. Optionally, the pyBacktrack output is merged with externally produced traditional paleobathymetry on subducted crust to obtain globally complete paleobathymetry grids. The procedure is implemented in `pybacktrack/paleo_bathymetry.py` and is exposed both as a command-line script (`python -m pybacktrack.paleo_bathymetry_cli`) and as a Python function (`pybacktrack.reconstruct_paleo_bathymetry_grids`). There are merged paleobathymetry grids available for the default plate model in pyBacktrack (Zahirovic 2022) for ages 0 to 170 Ma. They grid used in this paper is in the paleomagnetic reference frame (anchor plate *701701*). The exact paleomagnetic-reference-frame palaeobathymetry grids used in Figs. 2–4 are archived with the paper's reproducibility package (Müller et al., 2026b).

4.2 Cretaceous-Cenozoic paleobathymetry of the Atlantic-Tethys-Arctic realm

Time-dependent paleobathymetry grids are essential boundary conditions for paleoclimate models, biogeographic dispersal analyses and ocean-circulation reconstructions (Kennett, 1977; Sijp et al., 2014; Hutchinson et al., 2018; Lunt et al., 2021). We use the released pyBacktrack 1.5 paleobathymetry grids at 120, 80, 60 and 40 Ma to illustrate, respectively, the wide-open Cretaceous Tethys, the maximum extent of the Late Cretaceous oceans, the early Cenozoic Atlantic opening, and the mid-Eocene establishment of the modern Southern Ocean. The view is a Lambert azimuthal equal-area projection centred in the mid-North Atlantic (0 deg E, 45 deg N) with a 50 deg horizon cap. The visible region therefore covers the entire western Tethys (Mediterranean and Caribbean realm), the full North Atlantic, the Arctic Ocean (well past the pole) and extends south to roughly the equator; equal-area, so ocean-basin sizes can be compared visually without distortion.

https://doi.org/10.5194/egusphere-2026-3680
Preprint. Discussion started: 4 September 2026

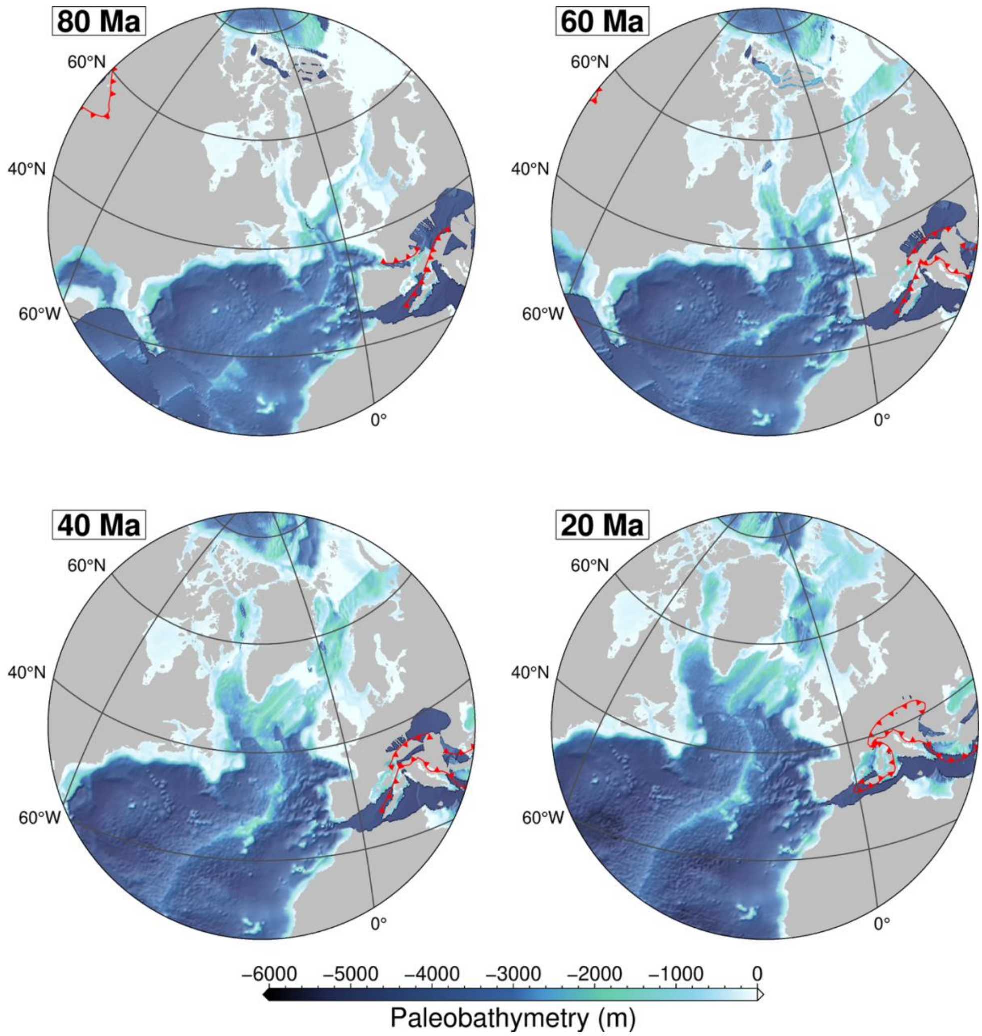

Figure 2. *Paleobathymetry from the pyBacktrack 1.5 at (a) 120 Ma, (b) 80 Ma, (c) 60 Ma and (d) 40 Ma. Reconstructed coastlines and plate boundaries and the underlying paleobathymetry grids are based on the Zahirovic et al. (2022) plate model in the paleomagnetic reference frame. Lambert azimuthal equal-area projection centred in the mid-North Atlantic (-20° E, 45° N) with a 50° horizon cap enabling regional ocean-basin comparison with minimal distortion.*

The four panels capture key Mesozoic-Cenozoic events of the North Atlantic and Tethyan systems: the deep central Atlantic conduit between a still narrow proto-North Atlantic and the southern Atlantic at 120 Ma; the equatorial Tethys deep seaway connecting the Atlantic and the Pacific realms at 80 Ma; the closing of the Western Interior Seaway and the opening of the Labrador Sea at 60 Ma; and, by 40 Ma, the constriction of the Tethys to its modern Mediterranean and Persian Gulf remnants while the North Atlantic and Norwegian-Greenland Sea reach near-modern bathymetric configurations.

https://doi.org/10.5194/egusphere-2026-3680
Preprint. Discussion started: 4 September 2026

4.3 Southern Ocean paleobathymetry through time

The southern high latitudes are central to Cenozoic climate evolution. Through the late Eocene the South Tasman Rise and the Tasmanian land bridge separated the proto-Indian Ocean from the proto-Pacific, and the Drake Passage between South America and the Antarctic Peninsula was either closed or shallow. The progressive subsidence of the South Tasman Rise from the late Eocene onward (Stickley et al., 2004; Bijl et al., 2013) and the deepening of the Drake Passage during the Oligocene-Miocene (Lawver and Gahagan, 2003; Eagles and Jokat, 2014) opened progressively deeper through-flows between the southern Atlantic, Indian and Pacific basins and established the conditions for the Antarctic Circumpolar Current (ACC). The ACC thermally isolates Antarctica from the warmer middle-latitude gyres, and the formation of a continuous, deep circum-Antarctic current is widely held to have triggered or amplified the onset of large-scale Antarctic glaciation at the Eocene-Oligocene boundary (Oi-1 event, ~33.7 Ma) (Kennett, 1977; Coxall et al., 2005; Houben et al., 2019), with the gateway depth playing a critical role in setting the strength of the ACC and therefore the magnitude of southward heat transport (Sauermilch et al., 2021). Reconstructing the bathymetry of these southern gateways through time is therefore a basic ingredient of any Cenozoic paleoclimate or paleocean-circulation model. We show pyBacktrack 1.5 grids at 35, 25, 15 and 0 Ma on a south-pole-centred orthographic projection (Fig. 3) to illustrate how the Southern Ocean bathymetric configuration evolved across this interval. The panels show the progressive opening and deepening of the Tasman Gateway, the opening of the Drake Passage, and the widening of the Southern Ocean, leading to the establishment of the modern circum-Antarctic deep water circulation.

https://doi.org/10.5194/egusphere-2026-3680
Preprint. Discussion started: 4 September 2026

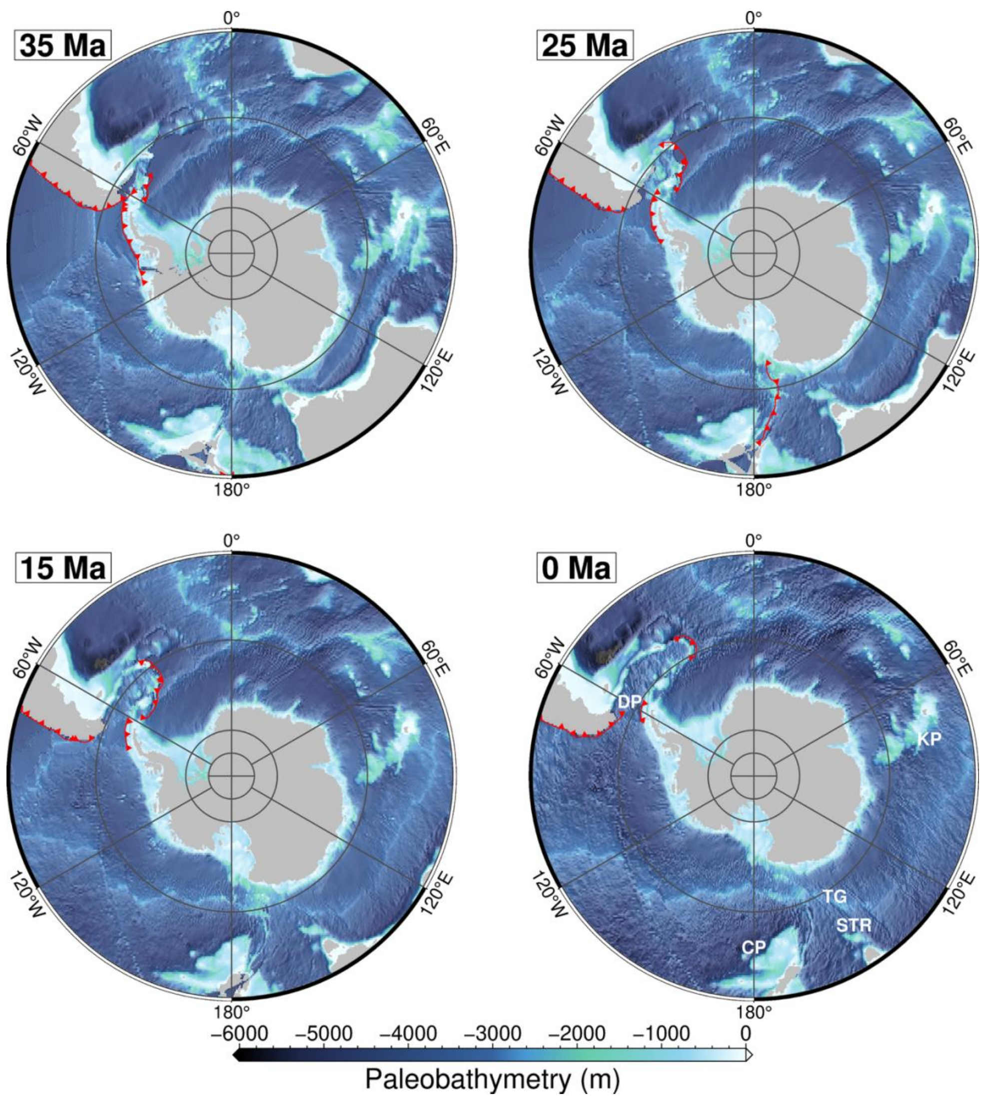

Figure 3. *Southern Ocean view of pyBacktrack 1.5 paleobathymetry at (a) 35, (b) 25, (c) 15 and (d) 0 Ma. The plate model used follows Fig. 2. White text acronyms are: DP – Drake Passage, KP – Kerguelen Plateau, TG – Tasman gateway, STR – South Tasman Rise, CP – Campbell Plateau. Lambert azimuthal equal-area projection centred on the south pole with a 50° horizon cap.*

4.4 Comparison with the Straume et al. (2020) Cenozoic forward-modelled paleobathymetry

We compare our pyBacktrack-derived paleobathymetry against independent grids whose methodology differs from ours in almost every respect. Straume et al. (2020) published a Cenozoic (1–65 Ma, 1 Myr) global paleobathymetry + paleotopography grid set with explicit emphasis on the Northern Hemisphere oceanic gateways. Their approach is a five-step forward physical model anchored at each time slice on the plate-kinematic reconstruction of Straume

https://doi.org/10.5194/egusphere-2026-3680
Preprint. Discussion started: 4 September 2026

et al. (2019), updated from Seton et al. (2012): (i) oceanic lithospheric age from the rotated age grid → basement depth from the Crosby and McKenzie (2009) thermal-subsidence formula; (ii) residual bathymetry of reconstructed large igneous provinces and microcontinents added on top; (iii) sediment thickness from an empirical age and latitude regression (Straume et al., 2019) with isostatic loading; (iv) regression-based continental margins with reverse-time sediment removal; (v) a global eustatic sea-level correction. Crucially, Straume et al. (2020) make explicit manual adjustments in four regional gateways — the Fram Strait, the Greenland–Scotland Ridge, the Tethys Seaway and the Central American Seaway — so that the modelled paleobathymetry honours geological and paleo-oceanographic constraints from the regional literature (e.g. Iceland mantle-plume support of the Greenland–Scotland Ridge, sub-aerial Hovgård microcontinent restricting Fram Strait deep-water exchange until the Early Pliocene).

pyBacktrack1.5 is fundamentally different. Rather than predicting depth at time t from a thermal-subsidence formula anchored on the plate reconstruction, the workflow takes the present-day age, sediment-thickness and bathymetry grids and back-tracks every submerged grid point through reversed subsidence, decompaction, sea-level and dynamic-topography corrections to the time of interest. Two consequences follow. First, the released pyBacktrack 1.5 grids reproduce whatever fine-scale fabric is present in the present-day source data on every patch of preserved crust — mid-ocean-ridge axes, fracture-zone offsets, abyssal-hill orientation, seamount provinces — in their kinematically reconstructed past positions, with no smoothing back to a formula. Second, the workflow is by construction unable to reconstruct bathymetry on seafloor that has since been subducted: it has no present-day grid point to back-track from. However, this is alleviated by merging pyBacktrack paleobathymetry for a forward model with some in-principle similarity to that used by Straume et al. (2020) for now subducted ocean crust. Straume et al. (2020), being a plate-reconstruction-driven forward model, suffers neither limitation — and applies manual gateway corrections on top — but at the cost of a smoother, globally-uniform-formula representation of basin-scale depth and a complete absence of the small-scale heterogeneity preserved by backtracking.

We compare the distribution of bathymetric values at each time slice using each product's own ocean mask. Figure 4 (top) shows the median ocean depth and the median ± 1 MAD (median absolute deviation; a robust analogue of standard deviation, in metres) envelope for both products through the 1-65 Ma common window; the bottom panel overlays the full depth-distribution histograms at 40 Ma. Three observations stand out: (a) the pyBacktrack reconstruction has a consistently shallower median ocean depth than Straume et al. (2020) by roughly 300-450 m through the Cenozoic, with the offset modestly larger in the Eocene; (b) the two products have comparable MADs (~970-1090 m for pyBacktrack, ~900-985 m for Straume), so the bulk shapes of the depth distributions are similar; and (c) the Straume reconstruction covers a slightly larger ocean-area fraction of its native grid (~0.70 vs ~0.66 for pyBacktrack), consistent with its ability to place depth on subducted seafloor and with its globally smoother continental-margin representation.

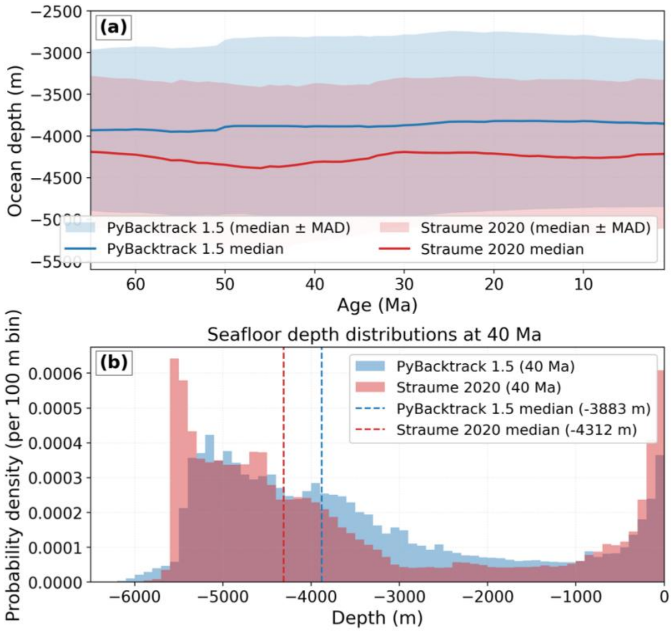

Figure 4. *Comparison of the pyBacktrack 1.5 paleobathymetry based on the (Zahirovic et al., 2022) plate model against the Straume et al. (2020) Cenozoic forward-model paleobathymetry over the common window 1-65 Ma. TOP: time-series of the median ocean depth (solid lines) and median ± 1 MAD (median absolute deviation, the robust analogue of standard deviation, in metres) envelope (shaded bands) for each product. BOTTOM: depth-distribution histograms at 40 Ma, with the per-product median marked as a dashed vertical line. Each product is summarised on its own ocean mask (PyBacktrack: cells where the grid is finite; Straume: cells where z < 0).*

The methodological and quantitative differences should not be read as one product being right and the other wrong. Each is fit for a different purpose. Straume et al.'s grids (2020) are suitable when the application is gateway-resolution paleo-ocean circulation modelling and when the user wants the benefit of literature-evaluated regional corrections. PyBacktrack is preferable when the application needs a self-consistent reconstruction whose physical assumptions can be audited end-to-end, or when the user wants the fine-scale fabric preserved on present-day-preserved crust, or when the analysis is augmented by individual wells where back-stripping is the appropriate tool. Merging the strengths of the two approaches — pyBacktrack-style back-tracking on preserved crust and Straume-style forward modelling on subducted crust — is our preferred method for complete paleobathymetry reconstruction.

4.5 NW Shelf data overview and well selection

For the regional and one-dimensional examples we use the Australian North West Shelf. The margin spans roughly 3000 km from the Carnarvon Basin in the southwest to the Browse Basin further north and the Bonaparte Basin in the Arafura Sea in the northeast (Fig. 5). It is one of the largest and most extensively drilled passive margins in the world. It developed through multiple Permian-Mesozoic rifting episodes including Permian-Triassic extension associated with the early break-up of Pangea, latest Triassic-Early Jurassic extension along what later became the western Australian margin, Late Jurassic-Early Cretaceous rifting and continental

https://doi.org/10.5194/egusphere-2026-3680
Preprint. Discussion started: 4 September 2026

break-up between Greater India and Western Australia, and the post-break-up opening of the Argo, Gascoyne, Cuvier and Perth abyssal plains (Gibbons et al., 2012, 2013). The Cenozoic record is dominated by passive thermal subsidence under a widespread carbonate platform that drowned and stepped down to the modern outer shelf during the Neogene. The NW Shelf is also a globally significant hydrocarbon province (Longley et al., 2002; Cathro et al., 2003), which is why an unusually dense industry-drilling effort has produced consistent, lithology-coded stratigraphy with paleobathymetry indicators derived from benthic foraminiferal assemblages - exactly the input that pyBacktrack needs. Its combination of long stratigraphic record, multi-phase tectonic history, dense well coverage, and well-resolved plate-tectonic context makes the NW Shelf an ideal natural laboratory for testing margin-scale backstripping workflows.

The well data used here (Fig. 5) were compiled by Müller et al. (2000). For the one-dimensional examples we feature a single long-record well, asteras, whose 20 stratigraphic horizons span 24 to 146 Ma, which is within the 0-150 Ma coverage of our preferred dynamic-topography model D10_gmcm9 (Braz et al., 2021) used in this context.

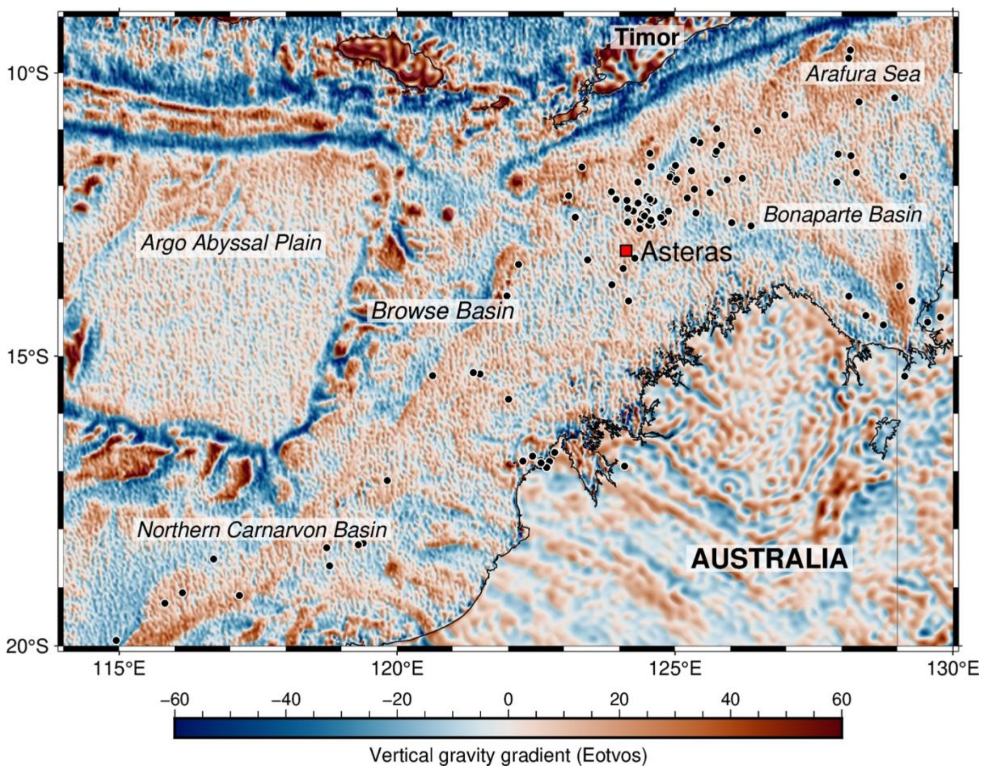

Figure 5. *Location map of 109 NW Shelf industry wells used in this paper compiled by Müller et al. (2000). Black dots mark the wells; the featured well, asteras, used for the one-dimensional examples (Figs. 6, 7 and 8) is highlighted with a red square and label. Background: Satellite vertical-gravity-gradient (Sandwell et al., 2014) exposes the structural fabric (rifted margins, fracture zones, abyssal-plain topography).*

4.6 Sea-level and dynamic-topography forcings used in backstripping

https://doi.org/10.5194/egusphere-2026-3680
Preprint. Discussion started: 4 September 2026

The tectonic subsidence inferred from well data depends on whether eustatic sea level fluctuations and/or mantle convection-driven dynamic topography through time is considered. Long-term eustatic sea level and dynamic topography via pyBacktrack as time series were sampled at the well location using the bundled Haq2024 long-term hybrid sea-level curve and the D10_gmcm9 dynamic-topography model of Braz et al. (2021), whose 0-150 Ma coverage spans the entire asteras stratigraphic record (oldest horizon 146 Ma). Figure 6 shows both forcings evaluated at the asteras location across the 150-0 Ma window used for every subsequent figure.

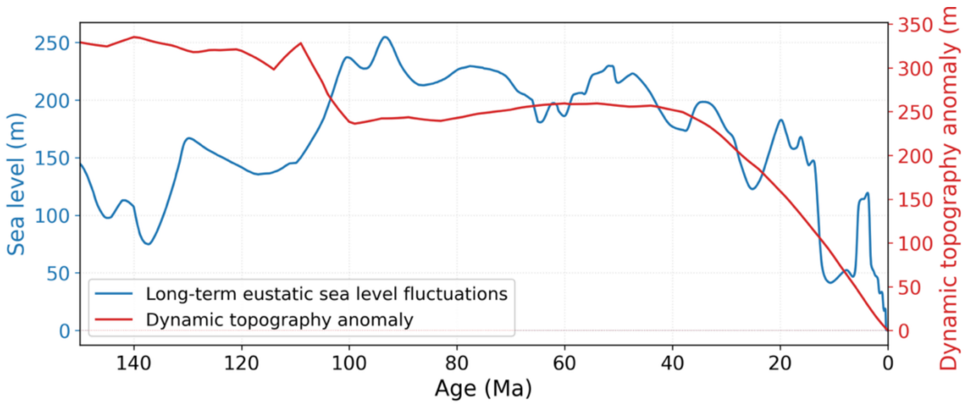

Figure 6. *Examples of eustatic sea-level and dynamic topography models at the featured NW Shelf well, asteras (see Fig. 5 for well site). Left y-axis: Haq2024 long-term sea-level curve as implemented in pyBacktrack 1.5 (Haq and Ogg (2024) (0–66 Ma), Haq (2014) (66-140 Ma) and Haq (2017) (140.1-150 Ma) (solid blue). Right y-axis: D10_gmcm9 dynamic-topography elevation anomaly at the well location relative to present (dashed orange; Braz et al., 2021).*

4.7 Backstripping in three configurations

Mirroring the bundled `pybacktrack/notebooks/backstrip.ipynb` workflow, we run `pybacktrack.backstrip_well` for the featured well asteras in three configurations: (a) no sea level and no dynamic topography (the raw decompacted record); (b) Haq2024 long-term hybrid sea level only, which isolates the eustatic correction; and (c) Haq2024 sea level together with the D10_gmcm9 dynamic-topography model of Braz et al. (2021), the full external correction set used throughout the rest of the paper. All three curves are overlaid on a single panel for direct comparison; each carries its min/max paleo-water-depth uncertainty envelope.

https://doi.org/10.5194/egusphere-2026-3680
Preprint. Discussion started: 4 September 2026

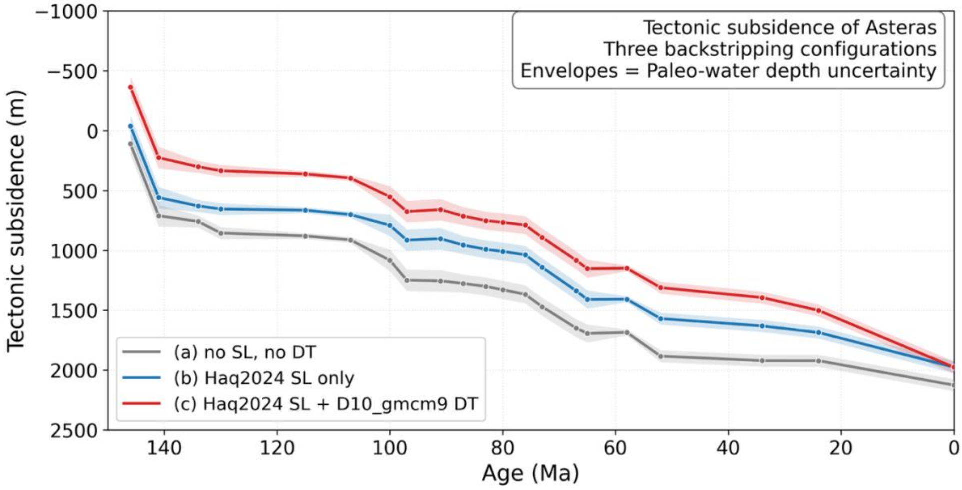

Figure 7. *Tectonic subsidence at industry well asteras, computed by pyBacktrack in three backstripping configurations overlaid on a single panel: (a) no sea level and no dynamic topography (grey); (b) Haq2024 long-term sea level only (blue); (c) Haq2024 sea level together with the D10_gmcm9 dynamic-topography model of Braz et al. (2021) (red). Shaded bands: min/max envelope implied by the paleo-water-depth uncertainty range in the well file. Markers: the twenty stratigraphic horizons at which the well is defined. Y-axis auto-scaled to the deepest envelope (positive-down); the top of the axis extends a small distance above present-day sea level so the configurations that briefly cross above zero in early history are not clipped.*

The well displays the characteristic two-stage subsidence pattern of a rifted passive margin: a rapid early phase in the Jurassic-Early Cretaceous and a more gradual post-rift thermal subsidence from the Late Cretaceous onward. The comparison between configurations (a), (b) and (c) shows that the eustatic correction has only a minor effect on the inferred tectonic subsidence (a few tens of metres over the well record), while the D10_gmcm9 dynamic-topography correction shifts the inferred subsidence by several hundred metres across the Cretaceous-Cenozoic interval where the model has its largest amplitude at this latitude. The width of the envelope is narrowest in well intervals constrained by shallow-shelf benthic assemblages and widest in the mid- to outer-shelf clay-dominated intervals - a direct visualisation of the most important uncertainty in 1D backstripping.

4.8 Geohistory analysis at the featured well

Geohistory or "Wheeler" diagrams visualise the through-time configuration of the sediment column relative to sea level, the sea floor and the basement. PyBacktrack returns, at each unit boundary, the decompacted thickness of every stratigraphic unit and the inferred water depth; we combine these to draw stacked, time-dependent stratigraphic units between the basement (tectonic subsidence) and the sea floor, following the structure of the bundled `geohistory_analysis.ipynb` notebook. The diagram is plotted in the standard geological positive-up sign convention: sea-level highstands plot above the zero datum, sea-floor and basement plot below it, and the dynamic-topography anomaly is shown relative to present.

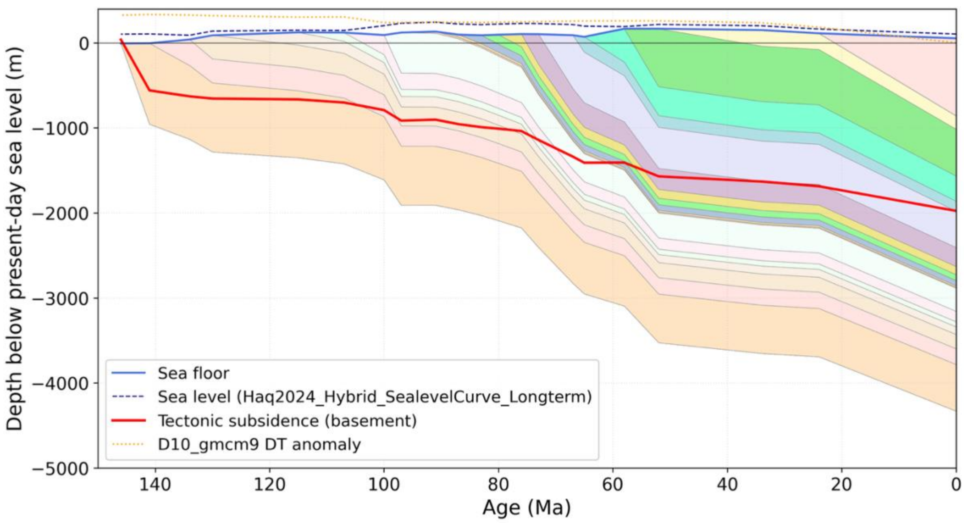

Figure 8. *Geohistory analysis of the featured well asteras. Coloured polygons show the decompacted thicknesses of the twenty individual stratigraphic units stacked downward from the time-dependent sea floor (royal-blue solid line). The dashed dark-blue line shows the Haq2024 long-term sea-level curve; the red line shows the basement (tectonic-subsidence) elevation; the dotted orange line shows the D10_gmcm9 dynamic-topography elevation anomaly relative to present (Braz et al., 2021).*

The geohistory diagram resolves the slow Cretaceous sedimentation episode and the relatively rapid Cenozoic carbonate-platform accumulation, with the sediment column thickening to modern values during the Neogene drowning of the shelf. The combined representation of sea-level curve, sea floor, basement and dynamic-topography anomaly makes the role of relative sea level in driving facies changes immediately legible, a feature that is particularly useful for teaching and outreach.

4.9 Gridded NW Shelf tectonic-subsidence rates

Generalising the one-dimensional workflow to all 109 NW Shelf wells lets us interpolate the inferred tectonic subsidence at any time slice into a margin-scale grid. To isolate the *rate* at which subsidence is accumulating, rather than its cumulative amount, we differentiate the per-well subsidence time-series with a forward 1 Myr finite difference and grid the resulting rate field. We do this in two configurations: (A) no sea level and no dynamic topography; and (B) the Haq2024 long-term hybrid sea level together with the D10_gmcm9 dynamic-topography model (Braz et al., 2021). The difference between the two rate fields quantifies how much of the apparent subsidence rate is absorbed by the combined eustatic + dynamic-topographic corrections.

At each time slice we grid the (lon, lat, rate) point cloud with the GMT *surface* algorithm under a tension of 0.5 (a balanced compromise between the pure minimum-curvature spline at T=0 and the pure harmonic solution at T=1) and clip the result with a concave-hull (alpha-shape) mask of the 109 well locations, dilated by 80 km, so that no extrapolation into the deep ocean or far into the Australian craton is produced. The well population thins back through time (109 wells at 50 Ma, 107 at 100 Ma, 68 at 200 Ma); we only generate grids for time slices where at least 10 wells contribute and the contributing wells span at least 3 degrees in longitude and

https://doi.org/10.5194/egusphere-2026-3680
Preprint. Discussion started: 4 September 2026

latitude. The oldest time based on this citerion is written by the workflow into `cutoff_time_Ma.txt`; the panels below are automatically clipped to this cutoff. The full workflow is implemented in `figures/scripts/07a_backstrip_all_nwshelf.py`.

A compact summary of the margin-scale rate behaviour is obtained by reducing the per-well rate point clouds to a time series of mean +/- one standard deviation across the contributing wells at every 1 Myr time slice (Fig. 9). Plotting both configurations on a single axis makes the magnitude of the eustatic + dynamic-topographic correction immediately visible as the displacement between the two mean curves; the shaded bands show the spread of subsidence-rate values across the NW Shelf at each Myr.

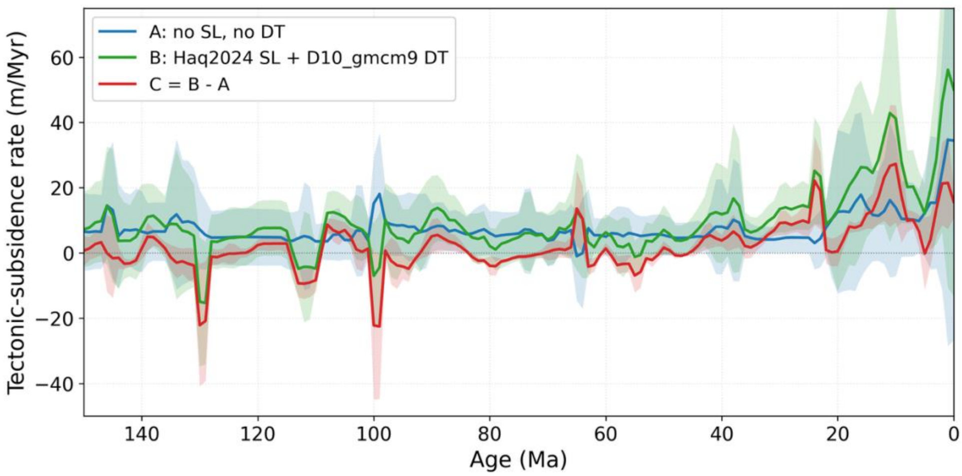

Figure 9. *Northwest Shelf tectonic-subsidence rate time series: across-well mean (solid line) +/- 1 standard deviation (shaded band) at every 1 Myr time slice for which at least 15 wells contribute, for configuration A (no sea level, no dynamic topography; blue), configuration C (Haq2024 long-term sea level + D10_gmcm9 dynamic topography, Braz et al., 2021; red) and the difference rate_D = rate_A - rate_C (green). Dashed grey line: zero rate (uplift above, subsidence below).*

https://doi.org/10.5194/egusphere-2026-3680
Preprint. Discussion started: 4 September 2026

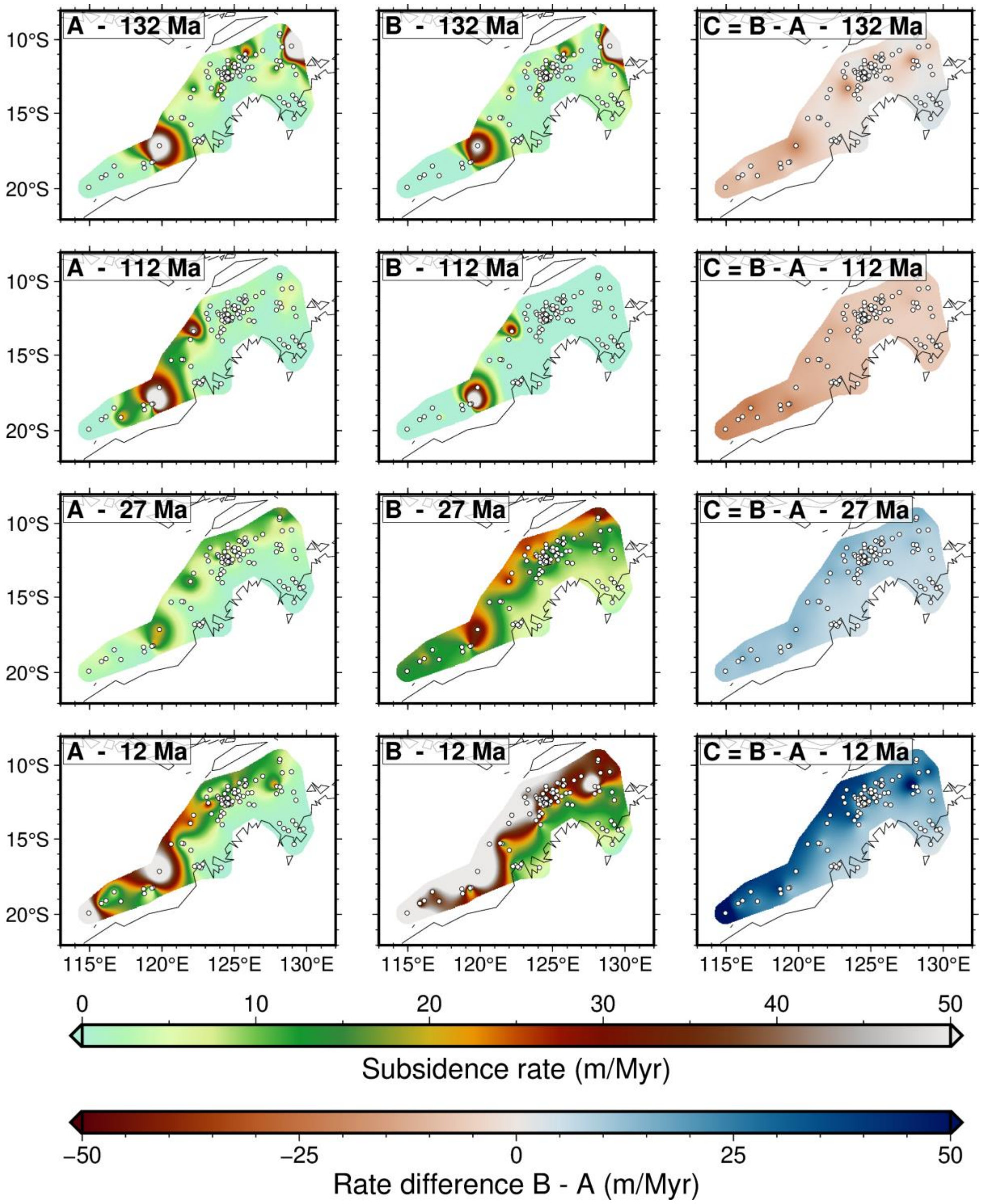

Figure 10. *Combined NW Shelf tectonic-subsidence rate fields at four selected 5 Myr intervals highlighted in Fig. 11(c) (centres 12, 27, 112 and 132 Ma) at which differences between tectonic subsidence rate without (A) and with (B) sea level and dynamic topography correction are maximised. Columns: (A) no sea level, no dynamic topography; (B) Haq2024 long-term hybrid sea level plus D10_gmcm9 dynamic topography (Braz et al., 2021); (C = B - A) the difference field. In column C, positive values (blue) denote excess subsidence introduced by the sea level and dynamic topography correction and negative values (warm) denote excess uplift. White-filled circles on every panel mark the 109 well locations. The rate field is*

https://doi.org/10.5194/egusphere-2026-3680
Preprint. Discussion started: 4 September 2026

interpolated with GMT `surface` (tension 0.5) and clipped to a concave-hull mask of the well distribution, extended by 80 km to create a buffer around the well data coverage.

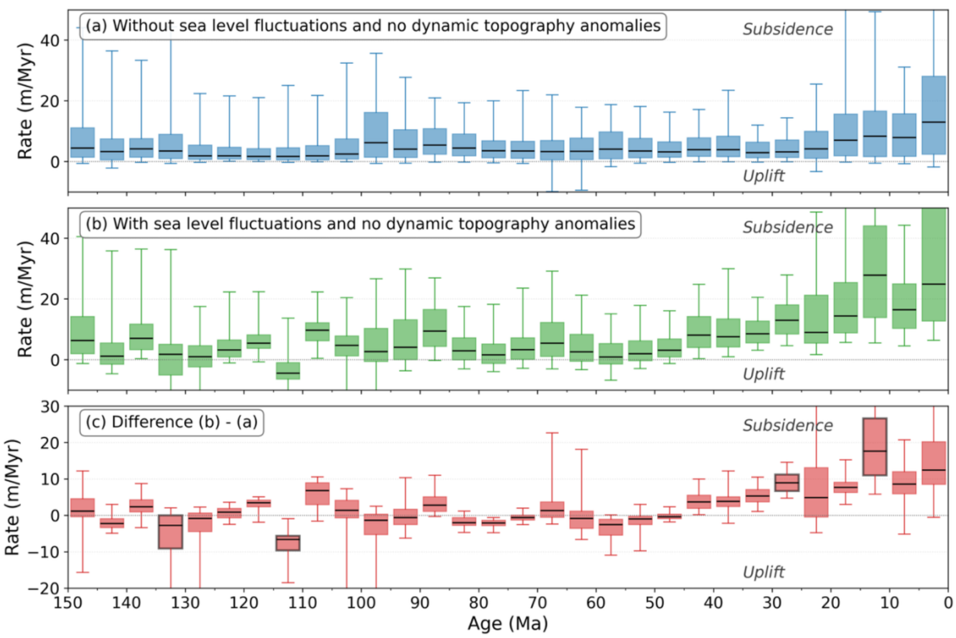

Figure 11. *NW Shelf tectonic-subsidence rate distribution through time, summarised as box plots at 5 Myr intervals. Three stacked panels: (a) configuration A (no SL, no DT); (b) configuration B (Haq2024 long-term hybrid sea level plus D10_gmcm9 dynamic topography, Braz et al., 2021); (c) the difference C = B - A. Each box pools every 1 Myr rate grid whose age falls inside the 5 Myr window, so each summarises spatial and within-interval temporal variability simultaneously. Box = inter-quartile range, central line = median, whiskers = 5th-95th percentile. The four boxes in panel (c) with thicker black edges (10-15, 25-30, 110-115 and 130-135 Ma) mark the five-Myr intervals with the largest mean |C|; their middle ages (12, 27, 112 and 132 Ma) are mapped in Figs. 10 and 12. Sign convention: positive = subsiding, negative = uplifting.*

The combined rate-field matrix and box plots (Figs. 10, 11) make the spatial pattern of the D10_gmcm9 dynamic-topography signal at the NW Shelf (Fig. 12) directly comparable to the well-based rate-difference field. The box-plot summary in Fig. 11 quantifies how the entire spatial distribution of the rate shifts when the SL + DT correction is applied, and identifies four 5 Myr intervals -- 10-15, 25-30, 110-115 and 130-135 Ma -- where this shift is largest (thicker-edged boxes in panel c). Each interval is mapped in Fig. 10 at its middle integer age (12, 27, 112 and 132 Ma), and the same four times are revisited in Fig. 12 to compare with the underlying DT field. Animations at 1 Myr resolution for the rate fields are produced by `10a_make_subsidence_videos.py` and are distributed alongside the paper.

4.10 Dynamic-topography

https://doi.org/10.5194/egusphere-2026-3680
Preprint. Discussion started: 4 September 2026

The tectonic subsidence difference field (Fig. 10, right column) shows how the modelled subsidence rate is altered when imposing combined sea-level and dynamic-topography correction at each pixel and each selected time, but the spatial structure is filtered through the distribution of the 109 NW Shelf wells. To complement this with a view that depends only on the dynamic-topography model itself, Fig. 12 plots the raw bundled D10_gmcm9 elevation anomaly (Braz et al., 2021) over the same NW Shelf region and at the same four selected times.

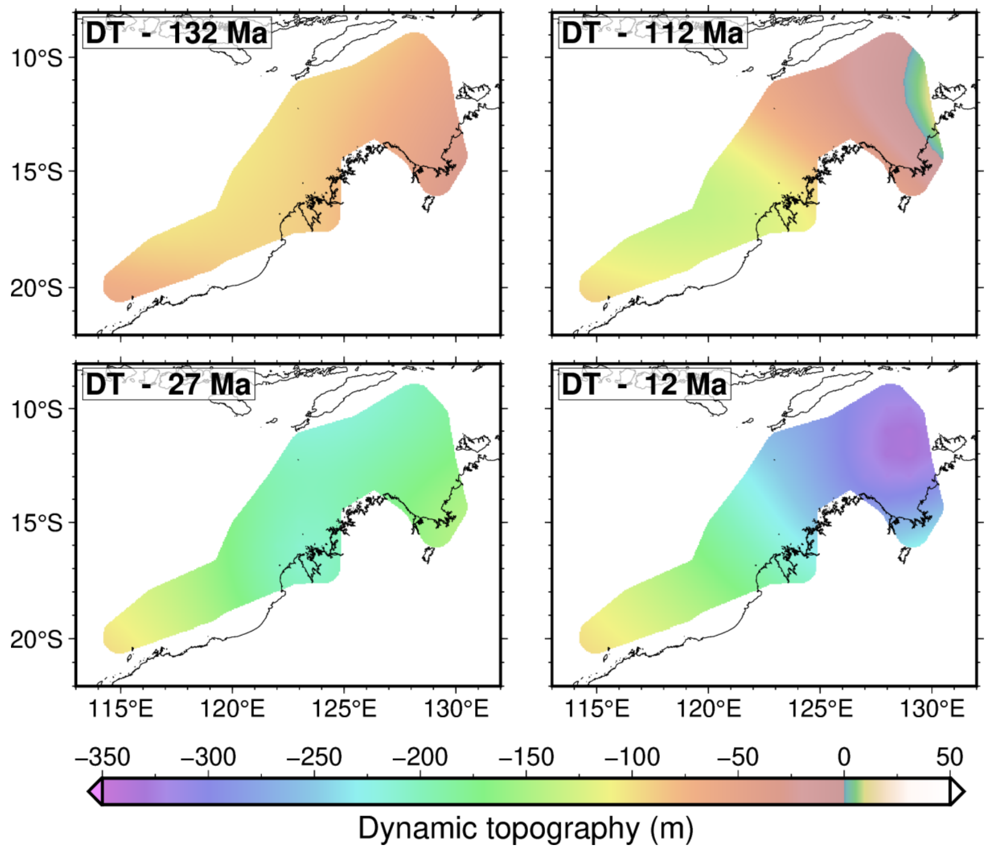

Figure 12. PyBacktrack-bundled D10_gmcm9 dynamic-topography elevation anomaly (Braz et al., 2021) over the NW Shelf at the same four times picked for Fig. 10: 12, 27, 112 and 132 Ma (top-left, top-right, bottom-left, bottom-right). Positive values (warm) denote locations that were higher than today (uplifted relative to present); negative values (cool) denote locations that were lower than today. The bundled 5 Myr DT grids are linearly interpolated in time and up-sampled to 0.05 deg through GMT `blockmedian` -> `surface` (tension 0.5), the same workflow used as for the well-based rate fields of Fig. 10. The same concave-hull mask of the 109 well locations is applied so the spatial footprint matches Fig. 10.

The dynamic topography fields are uniformly negative across the bulk of the NW Shelf, reflecting that the region is placed over a long-lived mantle downwelling, particularly in the last 100 Ma (Fig. 12). The amplitude and spatial extent of this negative anomaly migrate northeastward through the Cretaceous and intensify during the Cenozoic, consistent with Australia moving towards a subduction-related downwelling province.

https://doi.org/10.5194/egusphere-2026-3680
Preprint. Discussion started: 4 September 2026

5 Discussion

5.1 NW Shelf subsidence-rate variability and competing causes

The pyBacktrack 1.5 workflow lets us compare two alternative reconstructions of tectonic subsidence at the same well: configuration A, which ignores eustatic sea-level fluctuations and dynamic topography, and configuration B, which applies the Haq2024 long-term hybrid sea-level curve and the D10_gmcm9 dynamic-topography model (Braz et al., 2021). Each reconstruction is a model with its own shortcomings. On the one hand we know that long-term eustatic sea-level fluctuations and mantle-driven dynamic topography demonstrably influence shelf-scale paleo-water depths through time (Müller et al., 2008; Spasojevic and Gurnis, 2012; Haq and Ogg, 2024), so omitting them must introduce bias into the inferred tectonic subsidence. On the other hand the sea-level curve and the dynamic-topography model are themselves uncertain: eustatic reconstructions disagree on both amplitude and timing, and global mantle-flow models differ in their NW Shelf signature depending on assumed mantle viscosity structure, plate-motion history and initial condition. Configuration B is therefore not automatically the better estimate; if either correction is locally wrong, applying it adds noise rather than removing it.

Rather than attempt a full evaluation here, we ask a narrower, more tractable question: at the times when the sea level and dynamic topography correction has its largest effect on the inferred tectonic-subsidence rate on the NW Shelf, do independent geological constraints provide reasonable grounds to believe that configuration B is closer to the truth than configuration A? Ranking the 30 five-Myr intervals across 0-150 Ma by the spatial mean of the tectonic subsidence difference |C| = |rate_B - rate_A|, with a 15 Myr non-maximum suppression to avoid clustering in time, selects four intervals with rather different fingerprints in the Miocene, Oligocene and Cretaceous, highlighted as thicker-edged boxes in Fig. 11c. Their middle integer ages (12, 27, 112 and 132 Ma) are mapped in Figs. 10 and 12. The middle-Miocene interval dominates the ranking by a factor of 2-3 over the other three; the two Early Cretaceous intervals have comparable spatial means but very different spreads, which itself is diagnostic, as discussed below. We examine each interval in turn.

The 10-15 Ma interval (middle Miocene) has by far the largest mean |C| of the four (21.4 m/Myr -- more than twice the next-largest interval) and the highest IQR (16 m/Myr). Geologically, it coincides with foreland-style flexural loading driven by the collision of Australia with the Banda Arc and Timor (Müller et al., 2000; Cunneen et al., 2003; Harrowfield and Keep, 2005; Grahame and Cole, 2021). Broad-amplitude basement subsidence up to ~500 m has been documented inboard of the Timor Trough, propagating into the Roebuck, Browse, Vulcan and Argo-margin domains. Independently, Czarnota et al. (2013) document a regional pulse of accelerated subsidence near 9 Ma that they attribute to mantle convective drawdown, and Makuluni et al. (2022) and Young et al. (2020) link this Cenozoic acceleration to Australia's transit from an upwelling province to a subduction-related downwelling province above the southwest-Pacific slab system. Both flexural loading and mantle drawdown predict the kind of long-wavelength tectonic-subsidence anomaly that the D10_gmcm9 correction in configuration B explicitly removes. That a margin-wide ~20 m/Myr signal is large, regionally coherent (high IQR, comparatively low maximum-to-mean ratio of ~4-5) and aligned with two converging independent lines of evidence makes the middle Miocene the strongest a priori case for configuration B being closer to the true tectonic subsidence than configuration A.

The 25-30 Ma (latest Oligocene) interval has a mean |C| of 9.3 m/Myr, max |C| of 45 m/Myr and IQR of only 5 m/Myr -- a smaller-amplitude but still spatially organised signal. It coincides with the early stages of Australia's continental-scale tilt above the long-lived south-west Pacific

https://doi.org/10.5194/egusphere-2026-3680
Preprint. Discussion started: 4 September 2026

slab system (Müller et al., 2018; Makuluni et al., 2022; Young et al., 2020), a long-wavelength, low-frequency mantle-flow signal that drives gentle shelf-scale subsidence in the Northern Carnarvon Basin. The mantle-flow signature at this latitude in the D10_gmcm9 model has the appropriate sign and amplitude to capture this signal (Fig. 12, top-right panel). The supporting evidence is less pronounced than for the middle Miocene flexural-plus-drawdown case and the amplitude of the correction is smaller, but the consistency between the predicted continental-tilting direction and the D10_gmcm9 DT field offers reasonable grounds that configuration B is preferable here too.

The 110-115 Ma interval (Aptian) has the smallest IQR of the four (4 m/Myr) and the lowest max |C| (43 m/Myr) -- a flat, spatially uniform, low-amplitude signal. Geologically, Aptian-Albian to Cenomanian post-rift sequences in the Northern Carnarvon Basin are generally interpreted as a passive-margin succession of marine flooding, condensation, open-ocean circulation and thermal subsidence (Winata et al., 2023), with no compelling independent evidence for a discrete tectonic uplift pulse at ~110 Ma. The spatially uniform, low-IQR fingerprint is consistent with the absence of any distinct event: the modest mean |C| here is most plausibly the residue of long-wavelength differences between the SL and DT model outputs themselves rather than evidence of a real tectonic correction. In this interval neither configuration is strongly supported by external data and we cannot judge which is closer to the truth. This is the weakest of the four cases.

The 130-135 Ma (Hauterivian-Valanginian) interval has a mean |C| of 7.6 m/Myr but a max |C| of 94 m/Myr -- a maximum-to-mean ratio above 12, indicating that the signal is carried by isolated spikes rather than a regionally coherent trend. The IQR is intermediate (9 m/Myr). This statistical fingerprint matches the geological evidence remarkably well. Recent seismic-stratigraphic and burial-history work identifies multiple Early Cretaceous unconformities on the Gascoyne-Cuvier margin and the Northern Carnarvon Basin -- an intra-Valanginian unconformity at 134.98-133.74 Ma, a top-Valanginian unconformity at ~134-133 Ma, and an intra-Hauterivian unconformity at ~132.5-131 Ma (Reeve et al., 2022) -- and Valanginian uplift in the southern Exmouth Sub-basin beneath the KV seismic event (Longley et al., 2002). Independent compaction and vitrinite-reflectance modelling indicates removal of up to ~800 m of section from the flanks of the Exmouth, Barrow and Dampier sub-basins, attributed to depth-dependent extension and magmatic intrusion during the final stages of breakup between Australia and Greater India (Makuluni et al., 2024). These events fall directly within our 130-135 Ma box-plot interval, but they are intrinsically spatially heterogeneous: rift-flank uplifts vary at the structural-block scale, not at the long-wavelength scale at which dynamic-topography corrections operate (Reeve et al., 2022). The high-max, low-mean signature in Fig. 11(c) is therefore exactly what we would expect if the 132 Ma signal is a real but block-scale tectonic phenomenon that the long-wavelength dynamic topography correction cannot resolve. At face value the choice between A and B is therefore moe difficult to defend than for the Cenozoic intervals, although the spatial-statistical fingerprint helps with highlighting the underlying mechanism for observed tectonic subsidence anomalies at this time.

Taken together, the four largest-difference intervals span the full spectrum of confidence: a strong case for configuration B at 10-15 Ma (consistent independent evidence for both flexural loading and mantle drawdown); a reasonable case at 27 Ma (consistent with continental-tilting evidence at lower confidence); an unclear case at 112 Ma (no compelling independent evidence either way). and a weak case at 132 Ma (real but spatially heterogeneous rift-flank uplift not captured by long-wavelength DT models), The pyBacktrack 1.5 workflow is built to make this kind of honest comparison straightforward: producing the side-by-side A vs B time series, gridded rate fields and per-interval box-plot summaries takes minutes, and Fig. 11(c) localises the intervals where the question matters most.

5.2 Limitations and recommendations

Several limitations remain. PyBacktrack only generates paleobathymetry for crust that is preserved at present day; reconstructions of subducted crust must continue to be drawn from an external workflow and merged at output time. Continental subsidence is modelled with a single, uniform lithospheric stretching model that does not capture lithospheric heterogeneity, multiple rift episodes within a single basin, or the contribution of magmatic underplating. The dynamic-topography contribution remains uncertain at the few-hundred-metre level (Hoggard et al., 2017; Müller et al., 2018; Cao et al., 2019); the bundle of eight global models in pyBacktrack permits the user to characterise this uncertainty. The default lithology assumed in the paleobathymetry gridding workflow is `Average_ocean_floor_sediment`, which is appropriate for most of the open ocean but biases the decompacted thicknesses on shelves dominated by carbonate facies. Users requiring regional fidelity in those settings should override the default with the `-b` option or use a regional rift-grid file with locally appropriate lithology choices.

PyBacktrack 1.5 also makes more visible an issue that has long been implicit in 1D backtracking: the choice of dynamic-topography model can systematically shift paleo-water depths by several hundred metres. We recommend that users always compute their backtracked or backstripped results with at least two different dynamic-topography models from the eight bundled with pyBacktrack and report the resulting range as an additional source of uncertainty. Dynamic topography model-specific time limits are documented in the pyBacktrack reference documentation. All eight dynamic-topography models bundled with pyBacktrack, together with a growing library of additional published DT and plate-tectonic data sets, can be browsed interactively in 3D and downloaded from the GPlates Portal at https://portal.gplates.org (Müller et al., 2016a), so users can explore the model fields visually before choosing which to apply in pyBacktrack.

5.3 Current state and future development

PyBacktrack 1.5 represents a substantial generalisation of the original 1.0 tool from a one-dimensional drill-site backtracker to an integrated one- and two-dimensional paleobathymetry workflow. The new paleobathymetry gridding capability allows pyBacktrack to be used directly as a boundary-condition generator for climate, biogeographic and sedimentary-system models. The migration to Python 3 and to a multi-channel distribution (PyPI, conda-forge, Docker) lowers the barrier to use, and the move to a globally complete set of rift grids removes a common source of frustration when applying the package to user-supplied age or sediment-thickness grids.

Future development of pyBacktrack will focus on three areas: (i) incorporation of a workflow for generating paleobathymetry for now subducted crust; and (ii) introduction of probabilistic uncertainty propagation, so that the paleobathymetry grids carry per-grid-point uncertainty estimates derived from the uncertainties in the input present-day grids, the chosen subsidence model and the chosen dynamic-topography model.

6 Conclusions

PyBacktrack 1.5 is a major revision of the original pyBacktrack 1.0 community tool for reconstructing paleobathymetry on oceanic and continental crust. The package has been migrated to Python 3 and is now distributed via PyPI, conda-forge and Docker. The most significant scientific addition is the `paleo_bathymetry` gridding module, which reconstructs and backtracks every present-day submerged grid point to produce time-dependent, two-dimensional paleobathymetry grids that can be optionally merged with externally produced

https://doi.org/10.5194/egusphere-2026-3680
Preprint. Discussion started: 4 September 2026

grids for now subducted ocean crust. Default models have been updated to reflect a decade of community progress: the RHCW18 oceanic age-to-depth relationship, the Seton et al. (2020) age grid, the Straume et al. (2019) GlobSed sediment thickness grid and the Zahirovic et al. (2022) deforming plate model. PyBacktrack 1.5 supports both the mantle and paleomagnetic reference frames, ships globally complete rift start/end-age grids, and includes an expanded library of sea-level curves and lithology entries.

Code and data availability

PyBacktrack version 1.5.0 is archived at Zenodo (Müller et al., 2026a; https://doi.org/10.5281/zenodo.20809733) under the GNU General Public License v2.0. The code, locally held input data and figure-generation workflow used to produce the results in this paper are archived at Zenodo (Müller et al., 2026b; https://doi.org/10.5281/zenodo.20810168). This reproducibility package includes the tagged companion applications repository, the 109 Australian North West Shelf well files, regional vertical-gravity-gradient and D10_gmcm9 dynamic-topography data, dependency specifications, and the exact palaeobathymetry grids used for Figs. 2–4. The archived grid set spans 0–170 Ma and is based on the Zahirovic et al. (2022) deforming plate model in the paleomagnetic reference frame (anchor plate 701701). Provenance, licences and citation requirements for included data are documented in the archive.

Author contributions

RDM conceived the project, supervised the development of pyBacktrack 1.5, designed the application examples and drafted the manuscript. JC led the software engineering, implemented the paleobathymetry gridding module, the rift gridding scripts and the migration to Python 3, and produced the bundled documentation. SW and NMW contributed to algorithm design, and AD curated the lithology library. All authors contributed to interpretation and revision of the manuscript.

Competing interests

The authors declare that they have no competing interests.

Acknowledgements

PyBacktrack 1.5 was developed at the EarthByte Group, School of Geosciences, University of Sydney. We thank the broader pyGPlates and GPlates development community for their ongoing work that underpins pyBacktrack's reconstruction backbone, and we thank the numerous early users of pyBacktrack 1.0 whose feedback shaped the 1.5 release. This work was supported by the AuScope program of the Australian Government NCRIS initiative.

References

Allen, P. A. and Allen, J. R.: Basin Analysis: Principles and Applications, 2nd edn., Blackwell Publishing, Oxford, 549 pp., ISBN 978-0-632-05207-3, 2005.

Bijl, P. K., Bendle, J. A., Bohaty, S. M., Pross, J., Schouten, S., Tauxe, L., Stickley, C. E., McKay, R. M., Röhl, U., Olney, M., Sluijs, A., Escutia, C., Brinkhuis, H., and Expedition 318 Scientists: Eocene cooling linked to early flow across the Tasmanian Gateway, Proc. Natl. Acad. Sci. USA, 110, 9645-9650, https://doi.org/10.1073/pnas.1220872110, 2013.

https://doi.org/10.5194/egusphere-2026-3680
Preprint. Discussion started: 4 September 2026

Braz, C., Zahirovic, S., Salles, T., Flament, N., Harrington, L., and Müller, R. D.: Modelling the role of dynamic topography and eustasy in the evolution of the Great Artesian Basin, Basin Res., 33, 2466-2488, https://doi.org/10.1111/bre.12574, 2021.

Cao, W., Flament, N., Zahirovic, S., Williams, S., and Müller, R. D.: The interplay of dynamic topography and eustasy on continental flooding in the late Paleozoic, Tectonophysics, 761, 108-121, https://doi.org/10.1016/j.tecto.2019.04.007, 2019.

Cao, X., Flament, N., Müller, R. D., and Zahirovic, S.: The South China Block from the Jurassic to the present: kinematics, plate-boundary evolution and regional deformation, Earth-Sci. Rev., 220, 103744, https://doi.org/10.1016/j.earscirev.2021.103744, 2021.

Cathro, D. L., Austin, J. A. Jr., and Moss, G. D.: Progradation along a deeply submerged Oligocene-Miocene heterozoan carbonate shelf: How sensitive are clinoforms to sea level variations?, AAPG Bull., 87, 1547-1574, https://doi.org/10.1306/05210300177, 2003.

Colleoni, F., De Santis, L., Pochini, E., Forlin, E., Geletti, R., Brancatelli, G., Tesauro, M., Busetti, M., and Braitenberg, C.: PALEOSTRIPv1.0 - a user-friendly 3-D backtracking software to reconstruct paleo-bathymetries, Geosci. Model Dev., 14, 5285-5307, https://doi.org/10.5194/gmd-14-5285-2021, 2021.

Coxall, H. K., Wilson, P. A., Pälike, H., Lear, C. H., and Backman, J.: Rapid stepwise onset of Antarctic glaciation and deeper calcite compensation in the Pacific Ocean, Nature, 433, 53-57, https://doi.org/10.1038/nature03135, 2005.

Crampton, J. S., Cody, R. D., Levy, R., Harwood, D., McKay, R., and Naish, T. R.: Southern Ocean phytoplankton turnover in response to stepwise Antarctic cooling over the past 15 Myr, Proc. Natl. Acad. Sci. USA, 113, 6868-6873, https://doi.org/10.1073/pnas.1600318113, 2016.

Crosby, A. G.: Aspects of the relationship between topography and gravity on the Earth and Moon, PhD thesis, University of Cambridge, 2007.

Crosby, A. G. and McKenzie, D.: An analysis of young ocean depth, gravity and global residual topography, Geophys. J. Int., 178, 1198-1219, https://doi.org/10.1111/j.1365-246X.2009.04224.x, 2009.

Cunneen, J., Keep, M., and Crowe, W.: Early-stage orogenesis in the Timor Sea region, NW Australia, J. Geol. Soc. London, 160, 991-1001, https://doi.org/10.1144/0016-764903-020, 2003.

Czarnota, K., Hoggard, M. J., White, N., and Winterbourne, J.: Spatial and temporal patterns of Cenozoic dynamic topography around Australia, Geochem. Geophys. Geosyst., 14, 634-658, https://doi.org/10.1029/2012GC004392, 2013.

Dutkiewicz, A. and Müller, R. D.: The history of Cenozoic carbonate flux in the Atlantic Ocean constrained by multiple regional carbonate compensation depth reconstructions, Geochem. Geophys. Geosyst., 23, e2022GC010667, https://doi.org/10.1029/2022GC010667, 2022.

Eagles, G. and Jokat, W.: Tectonic reconstructions for paleobathymetry in Drake Passage, Tectonophysics, 611, 28-50, https://doi.org/10.1016/j.tecto.2013.11.021, 2014.

Gee, J. S. and Kent, D. V.: Source of oceanic magnetic anomalies and the geomagnetic polarity timescale, in: Treatise on Geophysics, vol. 5, Elsevier, 455-507, https://doi.org/10.1016/B978-044452748-6.00097-3, 2007.

Gibbons, A. D., Barckhausen, U., van den Bogaard, P., Hoernle, K., Werner, R., Whittaker, J. M., and Müller, R. D.: Constraining the Jurassic extent of Greater India: tectonic evolution of the West Australian margin, Geochem. Geophys. Geosyst., 13, Q05W13, https://doi.org/10.1029/2011GC003919, 2012.

Gibbons, A. D., Whittaker, J. M., and Müller, R. D.: The breakup of East Gondwana: assimilating constraints from Cretaceous ocean basins around India into a best-fit tectonic model, J. Geophys. Res. Solid Earth, 118, 808-822, https://doi.org/10.1002/jgrb.50079, 2013.

Grahame, J. and Cole, V.: Prospectivity of the Triassic successions of the North West Shelf of Australia: new insights from a regional integrated geoscience study, The Leading Edge, 40, 172-177, https://doi.org/10.1190/tle40030172.1, 2021.

Gurnis, M.: Phanerozoic marine inundation of continents driven by dynamic topography above subducting slabs, Nature, 364, 589-593, https://doi.org/10.1038/364589a0, 1993.

Haq, B. U., Hardenbol, J., and Vail, P. R.: Chronology of fluctuating sea levels since the Triassic, Science, 235, 1156-1167, https://doi.org/10.1126/science.235.4793.1156, 1987.

Haq, B. U.: Cretaceous eustasy revisited, Global Planet. Change, 113, 44-58, https://doi.org/10.1016/j.gloplacha.2013.12.007, 2014.

Haq, B. U.: Jurassic sea-level variations: a reappraisal, GSA Today, 28, 4-10, https://doi.org/10.1130/GSATG359A.1, 2018.

Haq, B. U. and Ogg, J. G.: Retraversing the highs and lows of Cenozoic sea levels, GSA Today, 34, 4-11, https://doi.org/10.1130/GSATGG593A.1, 2024.

Harrowfield, M. and Keep, M.: Tectonic modification of the Australian North-West Shelf: episodic rejuvenation of long-lived basin divisions, Basin Res., 17, 225-239, https://doi.org/10.1111/j.1365-2117.2005.00269.x, 2005.

Hoggard, M. J., White, N., and Al-Attar, D.: Global dynamic topography observations reveal limited influence of large-scale mantle flow, Nat. Geosci., 9, 456-463, https://doi.org/10.1038/ngeo2709, 2016.

Houben, A. J. P., Bijl, P. K., Sluijs, A., Schouten, S., and Brinkhuis, H.: Late Eocene Southern Ocean cooling and invigoration of circulation preconditioned Antarctica for full-scale glaciation, Geochem. Geophys. Geosyst., 20, 2214-2234, https://doi.org/10.1029/2019GC008182, 2019.

Hutchinson, D. K., de Boer, A. M., Coxall, H. K., Caballero, R., Nilsson, J., and Baatsen, M.: Climate sensitivity and meridional overturning circulation in the late Eocene using GFDL CM2.1, Clim. Past, 14, 789-810, https://doi.org/10.5194/cp-14-789-2018, 2018.

Jarvis, G. T. and McKenzie, D. P.: Sedimentary basin formation with finite extension rates, Earth Planet. Sci. Lett., 48, 42-52, https://doi.org/10.1016/0012-821X(80)90168-5, 1980.

Kennett, J. P.: Cenozoic evolution of Antarctic glaciation, the circum-Antarctic Ocean, and their impact on global paleoceanography, J. Geophys. Res., 82, 3843-3860, https://doi.org/10.1029/JC082i027p03843, 1977.

Kocsis, Á. T. and Scotese, C. R.: Mapping paleocoastlines and continental flooding during the Phanerozoic, Earth-Sci. Rev., 213, 103463, https://doi.org/10.1016/j.earscirev.2020.103463, 2020.

Lawver, L. A. and Gahagan, L. M.: Evolution of Cenozoic seaways in the circum-Antarctic region, Palaeogeogr. Palaeoclimatol. Palaeoecol., 198, 11-37, https://doi.org/10.1016/S0031-0182(03)00392-4, 2003.

Longley, I. M., Buessenschuett, C., Clydsdale, L., Cubitt, C. J., Davis, R. C., Johnson, M. K., Marshall, N. M., Murray, A. P., Somerville, R., Spry, T. B., and Thompson, N. B.: The North West Shelf of Australia - a Woodside perspective, in: The Sedimentary Basins of Western Australia 3, edited by: Keep, M. and Moss, S. J., Petroleum Exploration Society of Australia, Perth, 27-88, 2002.

https://doi.org/10.5194/egusphere-2026-3680
Preprint. Discussion started: 4 September 2026

Lunt, D. J., Bragg, F., Chan, W.-L., Hutchinson, D. K., Ladant, J.-B., Niezgodzki, I., Steinig, S., Zhang, Z., Zhu, J., Abe-Ouchi, A., et al.: DeepMIP: model intercomparison of early Eocene climatic optimum (EECO) large-scale climate features and comparison with proxy data, Clim. Past, 17, 203-227, https://doi.org/10.5194/cp-17-203-2021, 2021.

Makuluni, P., Hauser, J., and Clark, S. R.: Tilting of the Australian continent: new evidence from the subsidence and deposition history of the Northern Carnarvon Basin, Mar. Petrol. Geol., 143, 105784, https://doi.org/10.1016/j.marpetgeo.2022.105784, 2022.

Makuluni, P., Johnson, L. M., Langhi, L., Hauser, J., and Clark, S. R.: The spatio-temporal variation of exhumation and its impacts on the resource distribution in the Northern Carnarvon Basin, Australia, Mar. Petrol. Geol., 163, 106791, https://doi.org/10.1016/j.marpetgeo.2024.106791, 2024.

Mather, B. R., Müller, R. D., Zahirovic, S., Cannon, J., Chin, M., Ilano, L., Wright, N. M., Alfonso, C., Williams, S., Tetley, M., and Merdith, A.: Deep time spatio-temporal data analysis using pyGPlates with PlateTectonicTools and GPlately, Geoscience Data Journal, 11, 418-425, https://doi.org/10.1002/gdj3.185, 2024.

McKenzie, D. P.: Some remarks on the development of sedimentary basins, Earth Planet. Sci. Lett., 40, 25-32, https://doi.org/10.1016/0012-821X(78)90071-7, 1978.

Miller, K. G., Browning, J. V., Schmelz, W. J., Kopp, R. E., Mountain, G. S., and Wright, J. D.: Cenozoic sea-level and cryospheric evolution from deep-sea geochemical and continental margin records, Sci. Adv., 6, eaaz1346, https://doi.org/10.1126/sciadv.aaz1346, 2020.

Müller, R. D., Cannon, J., Williams, S., Dutkiewicz, A., and Wright, N. M.: PyBacktrack 1.5.0, Zenodo [software], https://doi.org/10.5281/zenodo.20809733, 2026a.

Müller, R. D., Cannon, J., Williams, S., Dutkiewicz, A., and Wright, N. M.: Reproducibility package for "PyBacktrack 1.5: A community tool for reconstructing paleobathymetry of drill sites, geohistory and global paleobathymetry", Zenodo [dataset], https://doi.org/10.5281/zenodo.20810168, 2026b.

Müller, R. D., Gaina, C., Tikku, A., Mihut, D., Cande, S. C., and Stock, J. M.: Mesozoic/Cenozoic tectonic events around Australia, in: The History and Dynamics of Global Plate Motions, edited by: Richards, M. A., Gordon, R. G., and van der Hilst, R. D., American Geophysical Union, Washington, DC, 161-188, https://doi.org/10.1029/GM121p0161, 2000.

Müller, R. D., Sdrolias, M., Gaina, C., and Roest, W. R.: Age, spreading rates and spreading asymmetry of the world's ocean crust, Geochem. Geophys. Geosyst., 9, Q04006, https://doi.org/10.1029/2007GC001743, 2008.

Müller, R. D., Qin, X., Sandwell, D. T., Dutkiewicz, A., Williams, S. E., Flament, N., Maus, S., and Seton, M.: The GPlates portal: cloud-based interactive 3D visualization of global geophysical and geological data in a web browser, PLoS ONE, 11, e0150883, https://doi.org/10.1371/journal.pone.0150883, 2016a.

Müller, R. D., Seton, M., Zahirovic, S., Williams, S. E., Matthews, K. J., Wright, N. M., Shephard, G. E., Maloney, K. T., Barnett-Moore, N., Hosseinpour, M., Bower, D. J., and Cannon, J.: Ocean basin evolution and global-scale plate reorganization events since Pangea breakup, Annu. Rev. Earth Planet. Sci., 44, 107-138, https://doi.org/10.1146/annurev-earth-060115-012211, 2016b.

Müller, R. D., Hassan, R., Gurnis, M., Flament, N., and Williams, S. E.: Dynamic topography of passive continental margins and their hinterlands since the Cretaceous, Gondwana Res., 53, 225-251, https://doi.org/10.1016/j.gr.2017.04.028, 2017.

https://doi.org/10.5194/egusphere-2026-3680
Preprint. Discussion started: 4 September 2026

Müller, R. D., Cannon, J., Williams, S. E., and Dutkiewicz, A.: PyBacktrack 1.0: a tool for reconstructing paleobathymetry on oceanic and continental crust, Geochem. Geophys. Geosyst., 19, 1898-1909, https://doi.org/10.1029/2017GC007313, 2018b.

Müller, R. D., Zahirovic, S., Williams, S. E., Cannon, J., Seton, M., Bower, D. J., Tetley, M. G., Heine, C., Le Breton, E., Liu, S., Russell, S. H. J., Yang, T., Leonard, J., and Gurnis, M.: A global plate model including lithospheric deformation along major rifts and orogens since the Triassic, Tectonics, 38, 1884-1907, https://doi.org/10.1029/2018TC005462, 2019.

Müller, R. D., Mather, B., Dutkiewicz, A., Keller, T., Merdith, A., Gonzalez, C. M., Gorczyk, W., and Zahirovic, S.: Evolution of Earth's tectonic carbon conveyor belt, Nature, 605, 629-639, https://doi.org/10.1038/s41586-022-04420-x, 2022.

Pälike, H., Lyle, M., Nishi, H., Raffi, I., Ridgwell, A., Gamage, K., Klaus, A., Acton, G., Anderson, L., Backman, J., et al.: A Cenozoic record of the equatorial Pacific carbonate compensation depth, Nature, 488, 609-614, https://doi.org/10.1038/nature11360, 2012.

Poblete, F., Dupont-Nivet, G., Licht, A., van Hinsbergen, D. J. J., Roperch, P., Mihalynuk, M., Johnston, S. T., Guillocheau, F., Baby, G., Fluteau, F., Robin, C., van der Linden, T. J. M., Ruiz, D., and Baatsen, M.: Towards interactive global paleogeographic maps, new reconstructions at 60, 40 and 20 Ma, Earth-Sci. Rev., 214, 103508, https://doi.org/10.1016/j.earscirev.2020.103508, 2021.

Reeve, M. T., Magee, C., Bastow, I. D., McDermott, C., Jackson, C. A.-L., Bell, R. E., and Prytulak, J.: Stratigraphic record of continental breakup, offshore NW Australia, Basin Res., 34, 226-254, https://doi.org/10.1111/bre.12611, 2022.

Richards, F. D., Hoggard, M. J., Cowton, L., and White, N.: Reassessing the thermal structure of oceanic lithosphere with revised global inventories of basement depths and heat flow measurements, J. Geophys. Res. Solid Earth, 123, 9136-9161, https://doi.org/10.1029/2018JB015998, 2018.

Richards, F. D., Hoggard, M. J., White, N., and Ghelichkhan, S.: Structure and dynamics of the oceanic lithosphere-asthenosphere system, Phys. Earth Planet. Inter., 309, 106559, https://doi.org/10.1016/j.pepi.2020.106559, 2020.

Sandwell, D. T., Müller, R. D., Smith, W. H. F., Garcia, E., and Francis, R.: New global marine gravity model from CryoSat-2 and Jason-1 reveals buried tectonic structure, Science, 346, 65-67, https://doi.org/10.1126/science.1258213, 2014.

Sauermilch, I., Whittaker, J. M., Klocker, A., Munday, D. R., Hochmuth, K., Bijl, P. K., and LaCasce, J. H.: Gateway-driven weakening of ocean gyres leads to Southern Ocean cooling, Nat. Commun., 12, 6465, https://doi.org/10.1038/s41467-021-26658-1, 2021.

Seton, M., Müller, R. D., Zahirovic, S., Gaina, C., Torsvik, T. H., Shephard, G. E., Talsma, A. S., Gurnis, M., Turner, M., Maus, S., and Chandler, M.: Global continental and ocean basin reconstructions since 200 Ma, Earth-Sci. Rev., 113, 212-270, https://doi.org/10.1016/j.earscirev.2012.03.002, 2012.

Seton, M., Müller, R. D., Zahirovic, S., Williams, S., Wright, N. M., Cannon, J., Whittaker, J. M., Matthews, K. J., and McGirr, R.: A global dataset of present-day oceanic crustal age and seafloor spreading parameters, Geochem. Geophys. Geosyst., 21, e2020GC009214, https://doi.org/10.1029/2020GC009214, 2020.

Sijp, W. P., von der Heydt, A. S., Dijkstra, H. A., Flögel, S., Douglas, P. M. J., and Bijl, P. K.: The role of ocean gateways on cooling climate on long time scales, Global Planet. Change, 119, 1-22, https://doi.org/10.1016/j.gloplacha.2014.04.004, 2014.

https://doi.org/10.5194/egusphere-2026-3680
Preprint. Discussion started: 4 September 2026

Spasojevic, S. and Gurnis, M.: Sea level and vertical motion of continents from dynamic earth models since the Late Cretaceous, AAPG Bull., 96, 2037-2064, https://doi.org/10.1306/03261211121, 2012.

Stein, C. A. and Stein, S.: A model for the global variation in oceanic depth and heat flow with lithospheric age, Nature, 359, 123-129, https://doi.org/10.1038/359123a0, 1992.

Stickley, C. E., Brinkhuis, H., Schellenberg, S. A., Sluijs, A., Röhl, U., Fuller, M., Grauert, M., Huber, M., Warnaar, J., and Williams, G. L.: Timing and nature of the deepening of the Tasmanian Gateway, Paleoceanography, 19, PA4027, https://doi.org/10.1029/2004PA001022, 2004.

Straume, E. O., Gaina, C., Medvedev, S., Hochmuth, K., Gohl, K., Whittaker, J. M., Abdul Fattah, R., Doornenbal, J. C., and Hopper, J. R.: GlobSed: updated total sediment thickness in the world's oceans, Geochem. Geophys. Geosyst., 20, 1756-1772, https://doi.org/10.1029/2018GC008115, 2019.

Straume, E. O., Gaina, C., Medvedev, S., and Nisancioglu, K. H.: Global Cenozoic paleobathymetry with a focus on the Northern Hemisphere oceanic gateways, Gondwana Res., 86, 126-143, https://doi.org/10.1016/j.gr.2020.05.011, 2020.

Uieda, L., Tian, D., Leong, W. J., Schlitzer, W., Toney, L., Grund, M., Jones, M., Yao, J., Magen, Y., Materna, K., et al.: PyGMT: A Python interface for the Generic Mapping Tools, Zenodo [software], https://doi.org/10.5281/zenodo.10578540, 2024.

Winata, M., Elders, C., Maselli, V., and Stephenson, R.: Regional seismic stratigraphic framework and depositional history of the post-Valanginian passive margin sequences in the Northern Carnarvon Basin, Northwest Shelf of Australia, Mar. Petrol. Geol., 152, 106225, https://doi.org/10.1016/j.marpetgeo.2023.106225, 2023.

Wright, N. M., Müller, R. D., Seton, M., Hosseinpour, M., and Williams, S. E.: Revised plate motions relative to the hotspots from global continental and oceanic moving hotspot reference frames, Geochem. Geophys. Geosyst., 16, 3709-3727, https://doi.org/10.1002/2015GC006019, 2016.

Young, A., Flament, N., Hall, L. S., and Merdith, A. S.: The influence of mantle flow on intracontinental basins: three examples from Australia, Basin Res., 33, 1429-1453, https://doi.org/10.1111/bre.12517, 2020.

Zahirovic, S., Eleish, A., Doss, S., Pall, J., Cannon, J., Pistone, M., Tetley, M. G., Young, A., and Müller, R. D.: Subduction kinematics and carbonate platform interactions, Geoscience Data Journal, 9, 371-383, https://doi.org/10.1002/gdj3.146, 2022.